

A new method for simulating multiple wind turbine wakes under yawed conditions

Dezhi Wei¹, Weiwen Zhao¹, Decheng Wan^{1*}, Qing Xiao²

¹Computational Marine Hydrodynamics Lab (CMHL), School of Naval Architecture, Ocean and Civil Engineering, Shanghai Jiao Tong University, Shanghai, China

²Department of Naval Architecture, Ocean and Marine Engineering, University of Strathclyde, Glasgow G4 0LZ, UK

* Correspondence author: dcwan@sjtu.edu.cn; Tel.: +86-21-3420-8437

Abstract: Counter-rotating vortices generated in wake steering not only deform the turbine wake, but also can make the wake trajectory of a non-yawed downwind turbine deviate from its rotor centerline, referred to as "secondary wake steering" phenomenon. Recent studies have also shown that the vortex interactions become clearer when the wind farm includes multiple turbines. However, in the common analytical models for active yaw control, the effects of these vortices are not considered. Evidently, this omission can lead to a decrease in model prediction accuracy. To compensate for it, a new analytical wind farm model is proposed. It adopts a physical-based momentum conserving wake superposition method to deal with the interaction of multiple wakes, in which, not only combining the streamwise velocity deficit of each individual yawed wind turbine, but also the transverse velocity from different wakes. Additionally, an "added yaw angle" is defined for a downwind turbine operating in upstream yawed turbine wakes, to reflect the change in local wind direction it perceives. For validation purposes, the LES wind field obtained from the SOWFA tool is used as a reference, and the newly proposed model is found to agree well with LES results and outperforms the representative conventional analytical model in almost all test cases. The new model can successfully reproduce the "secondary wake steering" phenomenon in the overlapped wake, and provides significant improvements in predicting power production of wind turbines.

Keywords: yawed wind turbine; secondary wake steering; momentum-conserving wake superposition method; added yaw angle

1. Introduction

Wake interaction is the main cause of power losses in wind farms, and it can lead to an increase in the fatigue loads of downwind turbines. Statistics have shown that the average annual loss caused by wakes may account for about 10% to 20% of the total power production [1]. In order to mitigate these adverse effects, researchers have developed some active wake control strategies. Some examples include [2-4], among which, the active yaw control is considered to be the most effective [5] and has received much attention. The idea behind such an operational control is to decrease the wake losses of the downstream turbines by intentionally altering the yaw angle of the controlled upwind turbine. By doing so, although the misaligned upstream wind turbine experiences an individual power loss, it can potentially increase the whole wind farm power production [6].

To apply active yaw control in real-world engineering, it is crucial to have a detailed understanding of the aerodynamic performance and wake flow behavior of yawed turbines. Focusing on a single horizontal axis wind turbine, Campo et al. [7] compared the difference of the aerodynamic loads exerted on the blade in yawed flow and axis flow. To systematically investigate the main turbine characteristics, Bastankhah and Porte-agle [8] performed several experiments on a three-blade wind turbine in a neutrally stratified boundary layer. The results indicated that, both power production and thrust force of the wind turbine decrease with increasing yaw angle, and a larger thrust coefficient was seen in the higher tip speed ratio. This is in agreement with other published researches [9,10]. In Lee et al. [11], they found that the yaw of wind turbine can not only

47 affect the development of a skewed wake structure, but also cause the cyclic variation in induced
48 velocity and aerodynamic load. What's more, van Dijk et al. [12] experimentally studied the effects
49 of yaw on power production and loads for full and partial wake overlap. In their studies, an increase
50 in the combined power production of the wind farm was seen when the upstream turbine yaws, and
51 the loads on the downstream turbine was reduced in partial wake overlap. Similar conclusions were
52 also drawn by Bartl et al [13]. More information on turbine thrust and power variation with the yaw
53 angle can be found in Ref. [14-16]. Additionally, by using large-eddy simulation, Jiménez et al. [17]
54 made an attempt to study the characteristics of wake deflection under different operating conditions,
55 and observed that it increases with yaw angle and thrust coefficient. Bartl et al. [18] investigated the
56 effect of inflow turbulence and shear on wake features behind a yawed turbine. In a LES study by
57 Vollmer et al.[19], the variation of wake shape and deflection magnitude with atmospheric stability
58 was discussed. Under uniform flow, Howland et al. [20] conducted a wind tunnel test on a porous
59 disk turbine with yaw angles. They used different method to quantify the wake center deflection, and
60 studied the formation of curled wake morphology, and attributed it to a pair of counter-rotating
61 vortices (hereafter CPV) that shed from the rotor plane. Later, in Bastankhah et al. [21], the potential
62 flow theory was applied to further analyze the mechanism of the "CPV". Apart from deforming the
63 wake, the impact of the counter-rotating vortices was seen to become clearer when the wind farm
64 includes multiple turbines [22,23]. The most important is that since the presence of these vortices, an
65 upstream yawed wake can deflect the wake of a downstream turbine, even if it is non-yawed. This is
66 called "secondary wake steering" phenomenon. The yawed wake combinations are also shown to
67 involve merging of generated cross flows, indicating that it is necessary to include the vortex
68 interactions for developing more effective wind farm controllers based on active yaw control.
69 Moreover, there are also some studies that focus on the possibilities of power optimization through
70 active yaw control. For example, in wind tunnel experiments, Bastankhah et al. [24] studied the
71 performance of a model wind farm with five turbine rows at various yaw angle distributions. They
72 found that the maximum total power enhancement can reach 17% for the tested wind farm, and
73 affected by the aforementioned vortex interactions, the optimal yaw angle distribution roughly
74 follows a linear relationship from front to rear turbine. A computational study by Gebraad et al. [25]
75 on six wind turbines also demonstrated the capability of active yaw control, in which, a 13% increase
76 of the combined power under yawed conditions was seen compared to the reference case with all
77 turbines aligned.

78 Besides high fidelity but costly numerical simulations and wind tunnel measurements,
79 researchers have also developed some analytical models for yawed wind turbine wakes. Due to the
80 advantages of simplicity and high efficiency, these models are widely used in engineering scenarios
81 requiring fast predictions. The first yawed wake model was proposed by Jimenez et al. [17], assuming
82 top-hat distributions of the streamwise velocity deficit and the skew angle. It is commonly used with
83 the wake recovery model of Jensen [26]. Despite its widely applications, the Jiménez model was found
84 to be inaccurate because the top-hat wake velocity deficit is not realistic [27]. In fact, the lateral profile
85 of normalized velocity deficit in the turbine wake approximately follows a self-similar Gaussian
86 distribution, which has been reported in many previous researches[28,29]. As such, several Gaussian-
87 based two dimensional (2D) analytical models were developed. One of the typical is derived by
88 Bastankhah et al. [21]. However, although its predictions show good agreement with the
89 experimental data, some of the model parameters are difficult to find universal values, their current
90 estimates greatly rely on numerical simulations or experiments. Consequently, the application of the
91 Bastankhah model is greatly restricted. The model of Dou et al.[30] also faces a similar dilemma. Later,
92 Qian et al. [31] developed a different Gaussian model for predicting wake velocity in the far-wake
93 region. In it, the input parameters are determined by ambient turbulence intensity and thrust
94 coefficient, which enhances the model applicability. But studies [27] shown that the Qian model tends
95 to underestimate the wake velocity deficit, especially for cases with small yaw angles. Adopting the
96 same assumptions as the Qian model, Wei and Wan [32] also derived an analytical model for yawed
97 turbine wakes, by incorporating the yaw effects into a classical Gaussian-based non-yawed wake
98 model. What's more, according to a relationship between the wake velocity components and the skew

99 angle, the Wei-Wan model is extended to incorporate the prediction on the transverse velocity, which
100 distinguish it from other common analytical models. More importantly, the model is simple in form,
101 only the wake width growth rate is required to be specified. More details about the Wei-Wan model
102 are given in Section 2.1 below.

103 Although some of these 2D models can accurately predict the wake behind a single yawed
104 turbine, their ability in modeling larger arrays of turbines implementing active yaw control is less
105 established. For example, in the study of Fleming et al. [22], the Gaussian model proposed by
106 Bastankhah et al. [21] was used together with the sum-of-squares (hereafter, SS) superposition
107 method [33] to predict the wake flow of a wind farm with multiple yaw wind turbines, but it was
108 found that there is a large difference between the model predictions and the LES results. A similar
109 phenomenon also appeared in Ref. [23]. We believe that there are two reasons for the above deviation.
110 First of all, the traditional wake superposition methods [33,34], represented by the SS used in Ref.
111 [22], are all empirical formulas without solid theoretical foundation, and the only distinction is that
112 the mathematical expressions are different. As pointed out by Crespo et al. [35], if not handled
113 properly, it may bring about unrealistic results. Secondly, as aforementioned, vortex interactions can
114 affect the wake steering performance, especially in cases with arrays of multiple turbines. However,
115 in the common analytical wind farm models for active yaw control, their effects are not considered.

116 The above deficiency motivates the development of new models, and one of the representatives
117 is the 3D analytical model proposed by Martínez-Tossas et al.[36]. Unlike the above-mentioned
118 conventional 2D analytical models, it takes no assumption on wake shape, nor does it use
119 superposition methods to describe the interaction effect of different wakes. Instead, it directly solves
120 a linearized version of the Navier–Stokes momentum equation with the curl effect, which makes it to
121 be able to capture the counter-rotating vortex pair in the wake flow of yawed wind turbines, and
122 further, successfully reproduce the secondary wake steering effect on a downstream wind turbine.
123 Despite of the merits, the available version of the 3D wake model is not mature enough at present,
124 some important factors are not being taken into account, such as the vortex decay effect and the added
125 turbulence generated by wind turbines. This results in some difference between the model prediction
126 and the real yawed wake flow. Furthermore, the RANS-like implementation of the 3D wake model
127 can increase the computation cost. Therefore, the 3D model is rarely used in engineering.

128 In contrast, although the conventional 2D wake models based on the geometrical deflection at
129 hub height cannot reconcile all observed phenomenon, it should be admitted that researchers in the
130 wind energy community have made a lot of efforts in that filed. They conducted a detailed and
131 valuable analysis of the yawed wake flow in the hub height plane. Therefore, if some improvements
132 are made to the existing analytical wind farm models based on the 2D models, for example, using a
133 physical-based wake superposition method and modeling the vortex interactions in wake
134 combination, the conventional analytical wind farm models may be revitalized. Fortunately, in a
135 recent paper by Zong et al. [37], they derived a novel wake interaction model, rigorously from the
136 law of conservation of momentum, referred to as "MC" model hereafter. It assumes that the total
137 velocity deficit in the overlapped wake is equal to a weighted sum of the velocity deficit for each
138 individual upwind turbine, rather than direct summation or square summation as in other common
139 wake superposition methods without theoretical justification; and the weights are expressed as the
140 ratio of the characteristic convection velocity of the individual wake to that of the overlapped wake.
141 Additionally, following the momentum conservation in spanwise, the MC model has also been
142 extended to combine the transverse velocity induced by yawed turbines, which make it possible to
143 reproduce the secondary wake steering effect crucial to active yaw control.

144 Due to the advantages of the MC model, we believe that it is a good choice for simulating the
145 superposed wakes of wind turbines operating in yawed conditions, although there is no relevant
146 practice so far. What's more, to better characterize the effects of the transverse velocity induced by
147 CPV in upstream yawed wakes, we introduce an "added yaw angle" to the wake-affected
148 downstream wind turbines, and it is defined as the ratio of the "equivalent lateral velocity" to the
149 "equivalent streamwise velocity" within the rotor area. Combining the above modules with the
150 Gaussian-based single wake model derived by Wei and Wan [32], a new analytical model for

151 simulating wind farm wakes under yawed conditions is formed. To evaluate the performance of the
 152 newly proposed model, it is compared against a conventional wind farm model, where the most
 153 commonly used sum of squares operation is adopted to combine the wakes. Note that, in the
 154 conventional model, only the streamwise velocity of each individual wind turbine is superimposed,
 155 excluding the transverse velocity as no superposition principle is given; of course, the "added yaw
 156 angle" is also not considered. For validation purposes, lots of numerical simulations are performed,
 157 on two-turbine arrays and three-turbine arrays with different yaw angle distributions, using the
 158 SOWFA tool; and the obtained wind turbine wakes are used as a reference to evaluate the analytical
 159 model predictions. Moreover, for a quantitative assessment, we also sample the averaged wind fields
 160 at different downwind locations using several virtual turbines, and calculate their power productions.
 161 The regression analysis of the streamwise wake velocity is also included in our study.

162 The remainder of this paper is organized as follows. In Section 2, a new analytical model for
 163 predicting wind farm wakes under yawed conditions is proposed. Then, descriptions of numerical
 164 experiments performed by the SOWFA tool and related analysis methodologies are given in Section
 165 3. By using the obtained LES wind field as a reference, in Section 4, the newly proposed model is
 166 evaluated and compared with a representative conventional analytical wind farm model. Finally,
 167 conclusions and future research are provided in Section 5.

168 2. Model description

169 In this part, a new method for modeling wind farm wake flows under yawed conditions is
 170 presented. Firstly, Section 2.1 briefly introduce the single analytical model applied to each wind turbine
 171 in the wind farm. Next, in Section 2.2, the wake superposition methods are given, used to describe the
 172 interaction mechanism of multiple wakes. In Section 2.3, an "added yaw angle" is defined for the
 173 downwind turbine operating in upstream yawed wakes. What's more, to close the analytical wind farm
 174 model, in Sections 2.4 and 2.5, methods used to estimate the local wake width growth rate and the
 175 aerodynamic performance of wind turbines are respectively illustrated in detail.

176 2.1. Single wake model

177 Due to the simplicity and the ability to reproduce various observations, in this study, the analytical
 178 wake model proposed by Wei and Wan [32] is adopted to predict the wake deflection and the far-wake
 179 velocity distributions for a single yawed wind turbine, including the streamwise velocity and the
 180 transverse velocity. It is a linear wake model derived from the conservation of mass and momentum,
 181 assuming the Gaussian profile for the streamwise velocity in the far-wake region.

182 In this analytical model, the equation for predicting streamwise velocity is written as:

$$\frac{u_w}{u_0} = 1 - \frac{C_T \cos \gamma}{16(k^* x/D + \varepsilon)^2} \times \exp\left(-\frac{1}{2(k^* x/D + \varepsilon)^2} \left\{ \left(\frac{z - z_h}{D}\right)^2 + \left(\frac{y - \delta}{D}\right)^2 \right\}\right) \quad (1)$$

183 where x , y , and z are streamwise, spanwise, and vertical coordinates, respectively; u_0 is the local
 184 wind speed perceived by the wind turbine, D is the rotor diameter, z_h is the turbine hub height, δ
 185 represents the wake center deflection, C_T and γ respectively denote the thrust coefficient and yaw
 186 angle of the wind turbine. k^* represents the wake width growth rate, which should be specified in
 187 advance for using the above equation, and discussions related to its value estimation can be found in
 188 Section 2.4 below. ε is a model parameter, determined by:

$$\varepsilon = 0.2\sqrt{\beta} \quad (2)$$

189 where β is a function of C_T , given by:

$$\beta = \frac{1 + \sqrt{1 - C_T \cos \gamma}}{2 \sqrt{1 - C_T \cos \gamma}} \quad (3)$$

190 What's more, the expression of the normalized wake center deflection is written as follows:

$$\frac{\delta}{D} = \theta_{c0} \frac{x_0}{D} + \frac{\sqrt{C_T / \cos \gamma} \sin \gamma}{23.866k^*} \times \ln \left| \frac{\left(\frac{\sigma_0}{D} + 0.166\sqrt{C_T \cos \gamma}\right) \left(\frac{\sigma}{D} - 0.166\sqrt{C_T \cos \gamma}\right)}{\left(\frac{\sigma_0}{D} - 0.166\sqrt{C_T \cos \gamma}\right) \left(\frac{\sigma}{D} + 0.166\sqrt{C_T \cos \gamma}\right)} \right| \quad (4)$$

191 Note that Equation (4) is only applicable to the far-wake region for $x > x_0$, where x_0 represents
 192 the onset of the far wake. In the near wake area for $x < x_0$, the wake deflection is assumed to be
 193 linear with the downstream distance, i.e., $\delta = \theta_{c0}x$, and the initial skew angle θ_{c0} can be calculated
 194 by the approach of Coleman et al. [38]:

$$\theta_{c0} = \frac{0.3\gamma}{\cos \gamma} (1 - \sqrt{1 - C_T \cos \gamma}) \quad (5)$$

195 The normalized wake width at $x = x_0$ is determined by:

$$\frac{\sigma_0}{D} = \sqrt{\frac{C_T (\sin \gamma + 1.978 \cos \gamma \theta_{c0})}{72\theta_{c0}}} \quad (6)$$

196 Based on the linear expansion assumption of the wake width, from Equation (6), result in:

$$\frac{x_0}{D} = \frac{(\sigma_0/D - \varepsilon)}{k^*} \quad (7)$$

197 Additionally, according to the relationship between the skew angle and wake velocity
 198 components, the transverse velocity in the far-wake region can be obtained, expressed as:

$$v = \frac{2.47C_T \sin \gamma u_w}{72(k^* x/D + \varepsilon)^2 - 1.978C_T \cos \gamma} \times \exp\left(\frac{(y - \delta + \sigma)/D}{2(k^* x/D + \varepsilon)}\right)^2 \quad (8)$$

199 2.2. Wake superposition models

200 As illustrated in Introduction, the downwind turbine inside a wind farm can be affected by
 201 multiple wakes from several upstream turbines. Therefore, when calculating the wake velocity at a
 202 certain downwind turbine location, the cumulative wake effects are supposed to be taken into
 203 account.

204 In previous analytical wind farm models, the sum of squares(SS) superposition method [33] is
 205 commonly used to multiple wakes, in which, the total wake velocity deficit is assumed as follows:

$$U_w(x, y, z) = U_0 - \sqrt{\sum_j^N (u_0^j - u_w^j(x, y, z))^2} \quad (9)$$

206 where j loops through all the turbines involved, N is the total number of the upwind turbines
 207 whose wake have effects on the target place, U_0 is the inflow velocity of the wind farm, u_0^j is
 208 the wind speed experienced by the j th turbine and u_w^j is the wind velocity due to the single wake from
 209 the turbine j .

210 Note that although the SS model is only an experience-based superposition method without
 211 definite physical basis, this does not prevent its extensive application in literature and commercial
 212 software. Hence, the SS, as a representative of most of the previous works in wind farm power
 213 prediction[39,40], provides a reference for assessing the performance of the newly proposed model.

214 Additionally, for the newly proposed wind farm model in this study, the momentum conserving
 215 wake superposition method[37] is adopted to deal with the interaction of multiple wakes. To apply
 216 it, the mean convection velocity for each individual wake should be calculated at first, which
 217 represents the spatially dependent wake velocity in the whole wake cross-section and is determined
 218 by:

$$u_c(x) = \frac{\iint u_w(x, y, z) \cdot u_s(x, y, z) dydz}{\iint u_s(x, y, z) dydz} \quad (10)$$

219 where u_s is the individual velocity deficit, defined as $u_s = u_0 - u_w$; and u_w is the corresponding
 220 streamwise velocity, can be calculated with Equation (1).

221 From Equations (1) and (10), yield:

$$\frac{u_c(x)}{u_0} = 1 - \frac{1}{\sqrt{2}} \times \frac{C_T \cos \gamma}{16(k^* x/D + \varepsilon)^2} \quad (11)$$

222 Following a similar procedure as the individual wake, the mean convection velocity for the
 223 overlapped wake (denoted by U_c) is defined as follows:

$$U_c(x) = \frac{\iint U_w(x, y, z) \cdot U_s(x, y, z) dydz}{\iint U_s(x, y, z) dydz} \quad (12)$$

224 where U_w is the combined wake velocity, given by:

$$U_w = U_0 - U_s \quad (13)$$

225 where U_s is the total velocity deficit in the superposed wake. To conserve the total momentum deficit
 226 in the streamwise direction during wake superposition, it has to satisfy the following expression:

$$U_s(x, y, z) = \sum_j^N \frac{u_c^j(x)}{U_c(x)} u_s^j(x, y, z) \quad (14)$$

227 Obviously, to solve U_c out of Equations (12) and (14), iterative calculations should be performed.
 228 Specifically, at first, assuming that U_c is equal to the maximum value of u_c^j , and then, estimate the
 229 total velocity deficit according to Equation (14); next, substitute the obtained U_s into Equation (12),
 230 to get the corrective value of the mean convection velocity for the combined wake U_c^* ; at last, let $U_c =$
 231 U_c^* , and repeat the above steps until the convergence criterion is met. In Zong et al.[37], the criterion
 232 is set to $|U_c - U_c^*|/U_c^* \leq 0.001$, which is also adopted in the present work. Under such condition, the
 233 calculation can usually reach convergence within 5 iterations.

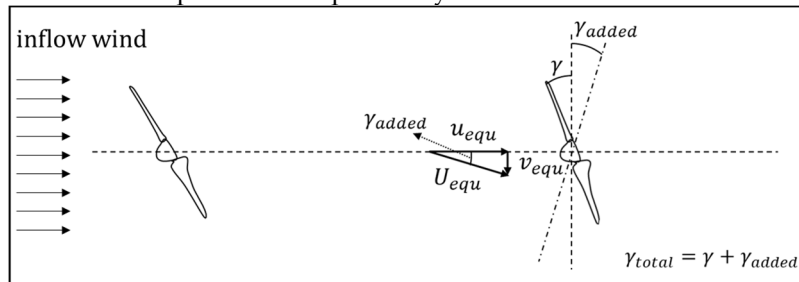
234 Analogous to Equation (14), following the momentum conservation in the spanwise direction,
 235 the total transverse velocity for the combined wake can be written as:

$$V(x, y, z) = \sum_j^N \frac{u_c^j(x)}{U_c(x)} v^j(x, y, z) \quad (15)$$

236 where v^j is the transverse velocity of the j th single wake, it can be found by Equation (8).

237 2.3. Definition of the "added yaw angle"

238 In order to better reflect the effects of transverse velocity induced by CPV in upstream yawed
 239 turbine wakes, a virtual "added yaw angle" is defined for the wake-affected downstream wind
 240 turbine, as shown in Figure 1. This is understandable since the upstream transverse velocity does
 241 change the local wind direction perceived by the downwind turbine. Therefore, when applying the
 242 single analytical model described in Section 2.1, a hypothetical yaw angle should be attached to the
 243 downwind turbine that overlaps with the upstream yawed wakes.



244 **Figure 1.** Schematic diagram of the "added yaw angle".

245 The “added yaw angle” (γ_{added}) is defined as an angle between the incoming wind direction and
 246 the equivalent resultant velocity (U_{equ}) acting at the rotor plane, it is composed of the equivalent
 247 transverse velocity (v_{equ}) and the equivalent streamwise velocity (u_{equ}), as presented in Figure 1.
 248 Specifically, in the calculation, first designate a number of sampling points in the rotor disk; then,
 249 extracting the wake velocity in each point and taking the average, thereby, the aforementioned
 250 equivalent values can be obtained:

$$u_{equ} = \sum_k^M u_k / M \quad (16)$$

$$v_{equ} = \sum_k^M v_k / M \quad (17)$$

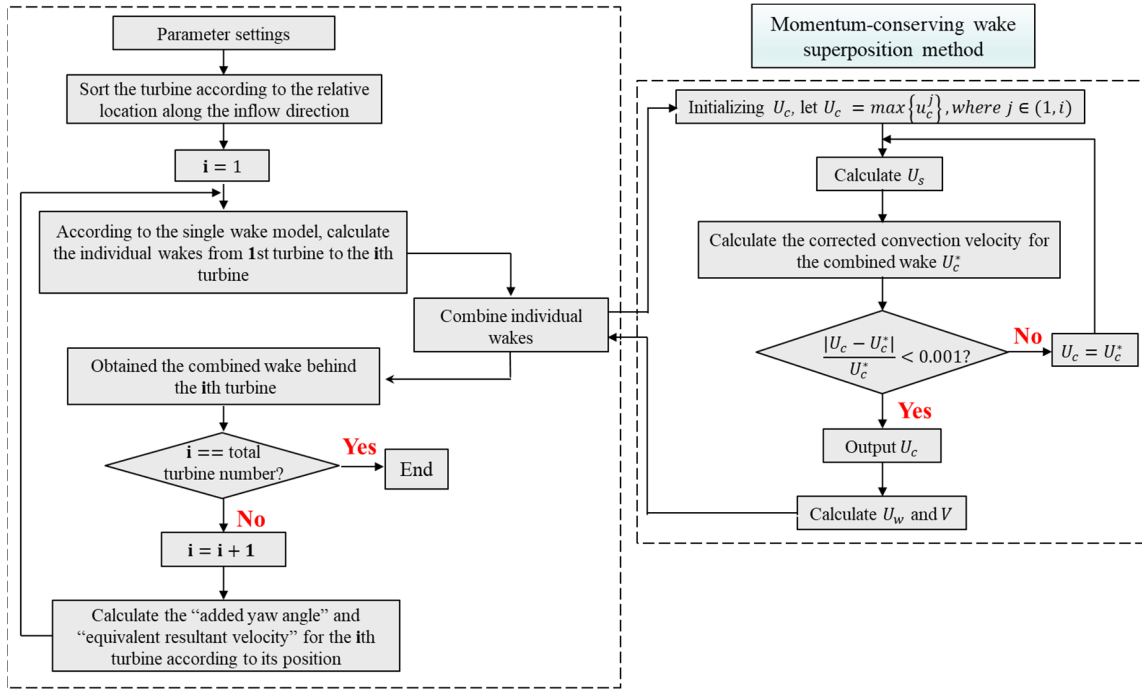
$$U_{equ} = \sqrt{u_{equ}^2 + v_{equ}^2} \quad (18)$$

$$\gamma_{added} = \arctan(v_{equ}/u_{equ}) \quad (19)$$

$$\gamma_{total} = \gamma_{set} + \gamma_{added} \quad (20)$$

251 where k is the index number, u_k and v_k are respectively the values of the streamwise and
 252 transverse wake velocity components at the k th point, they can be obtained by Equations (13) and
 253 (15); M is the total number of sample points. γ_{total} and γ_{set} in Equation (20) correspond to the total
 254 yaw angle perceived by the wind turbine and its set yaw value.

255 For the sake of clarity, Figure 2 shows a flow chart for modeling multiple wind turbine wakes
 256 under yawed conditions with the above-mentioned modules. The specific operations, in the order of
 257 execution, are described as follows. (1). Firstly, sort the wind turbines according to their relative
 258 locations along the inflow direction; (2). Starting the calculation from the most upstream turbine,
 259 apply the single analytical model to calculate the wake velocity components and the mean convection
 260 velocity for the individual wake at each downwind location; (3). In light of Equations (18) and (20),
 261 estimate the equivalent resultant velocity and the total yaw angle for the immediately adjacent
 262 downwind turbine; (4). Inserting the obtained values into the single wake model again, to predict the
 263 wake characteristics of the aforementioned downwind turbine in stand-alone conditions; (5) Deploy
 264 an iterative method to solve the mean convection velocity for the combined wake out of Equations
 265 (12) and (14), and then, by substituting the calculated U_c into Equations (14) and (15), the total
 266 streamwise velocity deficit and the total transverse velocity can be obtained. Obviously, this lay a
 267 foundation for predicting U_{equ} and γ_{total} of further downstream wind turbines; (6). Repeat steps 3
 268 to 5 until the last wind turbine, thus completing the wake modeling of the whole wind farm.
 269



270 **Figure 2.** Flow chart for modeling multiple wind turbine wakes under yawed conditions using the
 271 newly proposed model.

272 2.4. Turbulence intensity Model

273 For a wind turbine located in the combined wake of multiple upstream turbines, the local
 274 turbulence intensity it perceived includes not only the ambient turbulence intensity component, but
 275 also that generated by upwind turbines, referred to as “added turbulence intensity”[41,42]. What’s
 276 more, the wake width growth rate k^* in Equation (1) is known to be strongly affected by the
 277 turbulence intensity level [43]. Therefore, in order to better characterize the turbulence effects and
 278 improve the accuracy of wind farm power prediction, in here, following the work of Niayifar et al.[44],
 279 the wake width growth rate is no longer assumed to be constant, but expressed as a function of the
 280 local turbulence intensity at the wind turbine.

$$k^* = k_a \cdot I + k_b \quad (21)$$

281 where k_a and k_b are tuning parameters, and I is the local streamwise turbulence intensity
 282 immediately upstream of the target wind turbine. Note that, Equation (21) has been widely used in
 283 wind farm wake predictions [37,45] and achieved good results.

284 As illustrated above, the local streamwise turbulence intensity in the cumulative wake flows can
 285 be decomposed into two parts, given by:

$$I = \sqrt{I_0^2 + I_+^2} \quad (22)$$

286 where I_0 is the ambient turbulence intensity, I_+ is the added turbulence intensity induced by wind
 287 turbines.

288 For modeling I_+ in the far wake region, researches in the wind energy community have
 289 proposed several empirical equations [46,47]. In the internal tests, the Frandsen model [47] is found
 290 to be able to well simulate the mean added turbulence intensity after 5D downstream of the yawed
 291 wind turbine, and it is simple in form and has few input parameters. Consequently, in the present
 292 work, the Frandsen model is chosen to estimate the added turbulence intensity generated by wind
 293 turbines, it is expressed as:

$$I_+ = \sqrt{KC_T}/(x/D) \quad (23)$$

294 where K is a constant, set to 0.4.

295 In addition, from Ref.[44,48], the local turbulence intensity faced by a downwind turbine in the
 296 wind farm is largely affected by its surrounding upstream turbines, and the following method[44] is
 297 frequently used to calculate the added turbulence intensity at a given wind turbine (assuming its
 298 index number is i):

$$I_{+i} = \max \left(\frac{A_w^4}{\pi D^2} I_{+ji} \right) \quad (24)$$

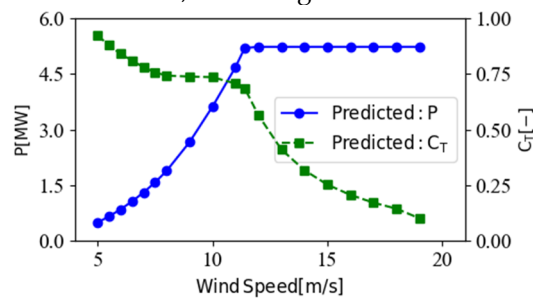
299 where I_{+i} is the added turbulence intensity perceived by the target turbine i , I_{+ji} is the added
 300 turbulence intensity generated by the upstream turbine j at the target turbine i , $\pi D^2/4$ and A_w are
 301 respectively the rotor area of turbine i and the overlap area between the i th turbine rotor plane and
 302 the wake of the j th turbine.

303 To calculate A_w in Equation (24), according to Niayifar et al.[44], a top-hat profile with a
 304 diameter of 4σ is assumed for the added turbulence intensity distribution, where σ is the standard
 305 deviation of the Gaussian-like velocity deficit profile, which is widely used as the characteristic wake
 306 width in previous studies[28,31,43].

307 2.5. Turbine model

308 As indicated by Equation (1), the thrust coefficient is an important input of the single wake model;
 309 power production is also a key indicator of the turbine performance. Hence, apart from the wake
 310 modeling module used to describe the wake characteristics, the wind turbine model should also be
 311 incorporated into the analytical wind farm model. Under non-yawed conditions, it is a common
 312 practice to plot the power and thrust coefficient curves as a function of the effective wind speed at
 313 the rotor, to predict the power production and thrust force corresponding to the local conditions the
 314 wind turbine is operating in [49,50].

315 The turbine used in the present work is the NREL 5-MW wind turbine, which is a three-blade
 316 upwind turbine with a rotor diameter of 126 m and a hub height of 90 m, and the reader can refer to
 317 Jonkman et al. [51] for more details on it. Additionally, the power and thrust coefficient curves of the
 318 NREL 5-MW turbine are shown in Figure 3. Note that the drawing data are derived from internal
 319 numerical simulations, may be slightly different to the results calculated by FAST [52], as only the
 320 rotor blades are modeled in the simulations, excluding tower and nacelle.



321 **Figure 3.** Simulated power and thrust coefficient curves with respect to the wind speed for the NREL
 322 5-MW wind turbine.

323 When the wind turbine yaws, due to the reduction in the effective inflow speed and the rotor
 324 frontal area, a drop is seen in power output and thrust force [8,9,10,53]. Therefore, in order to
 325 accurately predict the power and thrust of the yawed wind turbine, it is important to establish a
 326 reliable model to reflect the effect of yaw on the aerodynamic performance, and researchers have
 327 done lots of relative studies. For example, in actuator disk theory [54], assuming that only the normal
 328 velocity component crosses the rotor plane. For a yawed wind turbine, the axial inflow component it
 329 perceives is quite different from that of a non-yawed turbine, and in geometric, the two are in a cosine
 330 relationship, so:

$$P = P_0 \cdot \cos^3 \gamma \quad (25)$$

$$T = T_0 \cdot \cos^2\gamma \quad (26)$$

331 where P and T denote the power and thrust force under yawed conditions; P_0 and T_0 are the
332 power and thrust force at zero yaw.

333 However, it should be mentioned that multiple factors can affect the performance of the yawed
334 turbine, for instance, the turbine type and operating conditions [10,53]. Consequently, the above
335 relationships have not been widely recognized, although they are supported by some experimental
336 results [55]. Additionally, in the Ref. [10,56], it was observed that the power of a yawed turbine was
337 proportional to the square of cosine of yaw angle; and in Zong et al. [9], a $\cos^{1.8}\gamma$ shape was found
338 to fit the $C_T - \gamma$ curve. In conclude, it is difficult to find unanimous statement about the relationships
339 between power, thrust and yaw angle.

340 To achieve the goal of accurately predict the steady-state aerodynamic performance of a yawed
341 wind turbine at different operating conditions, Dahlberg and Montgomery [57] proposed the
342 following method, in which, tunable parameters are introduced to match the power and thrust loss
343 caused by yaw:

$$P = P_0 \cdot \cos^p\gamma \quad (27)$$

$$C_T = C_{T0} \cdot \cos^q\gamma \quad (28)$$

344 where C_{T0} represents the thrust coefficient at zero yaw; p and q are tunable parameters.

345 Due to the flexible of the Dahlberg's method, it is adopted in the present work, and the values of
346 the tunable parameters are determined by fitting the numerical simulation data for the NREL 5MW
347 wind turbine at different yaw angles. More details are shown in Section 4.1 below.

348 3. Wake simulations

349 To assess the performance of different analytical wind farm models for active yaw control, a
350 number of numerical simulations for wind turbines with different yaw angle distributions are
351 performed using the SOWFA tool, and the obtained LES wind field is used as a reference. The
352 numerical setting of the test cases is described in Section 3.1, and then, some analysis methods for
353 assessing analytical model predictions are given in Section 3.2.

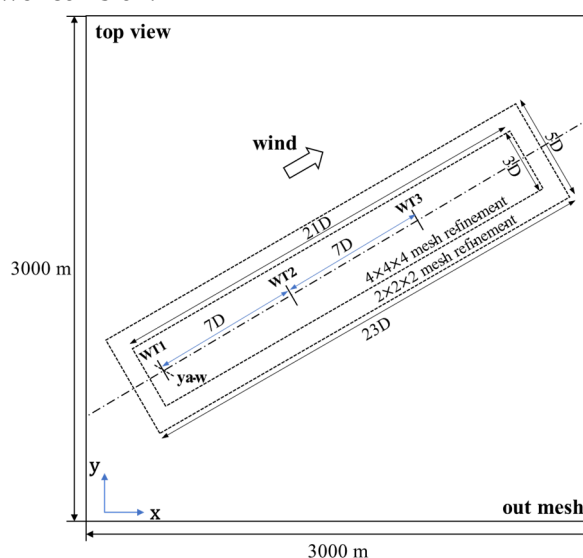
354 3.1. Numerical setup and test cases

355 The numerical simulations are conducted using the Simulator for Wind Farm Applications
356 (SOWFA) from the National Renewable Energy Laboratory (NREL), which is a high-fidelity tool for
357 investigating the wind turbine performance and wake characteristics. Within SOWFA, the LES
358 technique is applied to solve the filtered Navier–Stokes equations, and the contribution of the sub-
359 grid scales to the resolved flow field is parameterized by the eddy-viscosity model. In particular, the
360 governing equations are discretized using an unstructured, collocated, finite-volume formulation,
361 and the time discretization is second-order backward. Additionally, the actuator line method [58] is
362 introduced to model the turbine-induced forces for improving computational efficiency, which was
363 widely used in previous and its effectiveness has been validated [5,28]. More details on the SOWFA
364 tool can be found in Ref. [59].

365 In the current study, at first, several numerical simulations on a single wind turbine are
366 conducted, with the yaw angle being 0° , 10° , 20° and 30° , respectively. Next, to provide a reference
367 wind field for the analytical model predictions, four test cases are considered, including three two-
368 turbine arrays and a three-turbine array, where the streamwise spacing between two consecutive
369 turbines is 7 rotor diameters. In the test cases one, two and three, the first wind turbine is operating
370 with 10° , 20° and 30° yaw misalignment, respectively; and the second turbine is maintained non-
371 yawed. In the fourth case, three tandem-arranged wind turbines are tested, with the most upstream
372 turbine being yawed 20° . What's more, to evaluate the predictive performance of analytical models
373 on power output, another several two-turbine scenarios are simulated where the front turbine is
374 yawed 20° and the yaw angle of the second turbine is varied through a range of -15° and $+15^\circ$.

375 Specifically, the numerical simulation of each test case is divided into two stages. Firstly, a
 376 precursor simulation without wind turbines is performed to generate a realistic neutral boundary
 377 layer(NBL). The computational domain size is 3000 m×3000 m×1000 m, and it is discretized into
 378 300×300×100 grid points. All lateral boundaries in this simulation stage are periodic, and the
 379 horizontally mean wind speed at turbine hub height is driven to 8 m/s. What's more, the surface
 380 aerodynamic roughness height and the potential temperature rate are respectively set to 0.001 m and
 381 0 K/m, typical of the offshore conditions. In a whole, the setting is the same as that in Ref. [59], because
 382 the inflow it generates has been validated and represents a realistic scenario. The precursor
 383 simulation first ran for 18000 s, to ensure reaching a quasi-steady condition; and then, it ran for
 384 another 2000 s, and during that time, the relevant flow variables on the upstream boundary were
 385 stored at every time step, which would be enforced as the inflow boundary condition in the next
 386 simulation stage.

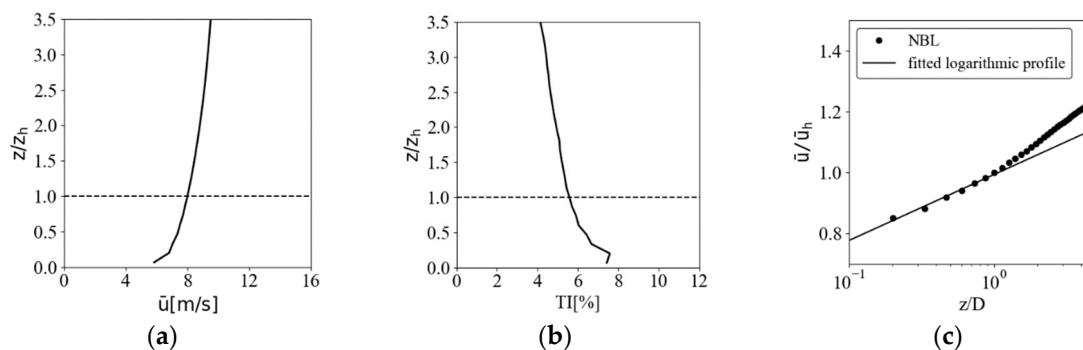
387 In the second stage, the wind turbines are immersed in the flow field. The boundary conditions
 388 in this simulation stage are different from the precursor simulation. In particular, only the side
 389 boundaries are periodic; for the upstream boundary condition, it is specified using the saved plane
 390 of turbulent data; and on the downstream boundary, the gradient of velocity and temperature are
 391 taken to be zero so that the turbine-induced wakes can exit without cycling back. What's more, we
 392 locally refined the mesh around the wind turbines and their wakes so as to gain the resolution
 393 required to capture the wake structures. Details on the positioning of the turbine and meshing of the
 394 domain are presented in Figure 4. For each test case, the second stage simulation ran for 2000 s, but
 395 only the simulated data in the last 1200 s was extracted and averaged to eliminate the transient effects.
 396 Moreover, it should be mentioned that, in order to exclude the additional wake deflection arising
 397 from the vertical momentum, no vertical tilt is applied to the turbine rotor in the numerical
 398 simulations, although in fact, the NREL 5-MW wind turbine used in the present work has a 5° shaft
 399 tilt to avoid the blade-tower collision.



400

401 **Figure 4.** Schematic on the positioning of the turbine and meshing of the domain. D represents the
 402 rotor diameter. WT1, WT2, and WT3 are the names of wind turbines.

403 Figure 5 presents the statistical features of the inflow generated in precursor simulation stage.
 404 The vertical profiles of the normalized streamwise inflow velocity and the streamwise turbulence
 405 intensity are shown in Figure 5(a) and (b). It can be seen that, the mean incoming wind speed and the
 406 turbulence intensity at hub height are around 8 m/s and 5.6%, respectively. In addition, to further
 407 assess the simulated boundary layer flow, we plot the measured streamwise velocity profile and the
 408 perfect logarithmic velocity profile on a semi-log scale in Figure 5(c). Apparently, below
 409 approximately 100 m, corresponding to the position of $z/D = 10^0$ in the x label, the measured inflow
 410 velocity profile substantially satisfies the law of the wall scaling, indicating that the desired inflow
 411 condition can be well generated in the precursor simulation.



412 **Figure 5.** Main features of the incoming flow: vertical profiles of (a) the normalized streamwise inflow
 413 velocity and (b) the streamwise turbulence intensity. The horizontal dashed line indicates the hub
 414 height level; (c) vertical profile of the normalized streamwise inflow velocity on a semi-log scale. The
 415 black solid line represents perfect law-of-the-wall scaling.

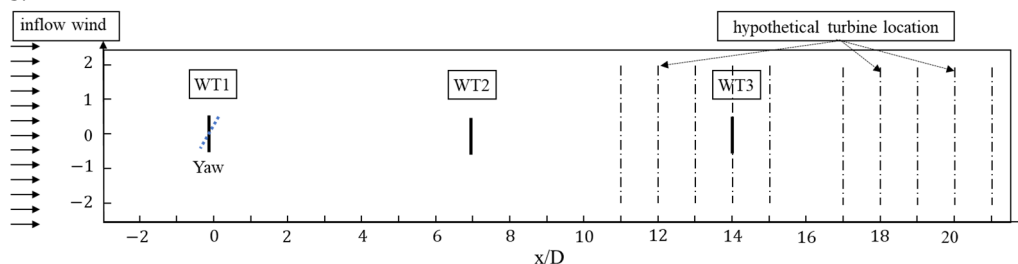
416 3.2. analysis methods

417 In order to better evaluate the performance of different wind farm wake models, we introduce
 418 two analysis methods in the present work. The first one is the linear regression analysis. To be specific,
 419 based on the wake flow data obtained from both the LES wind field and the analytical model, we can
 420 get a fitted regression line reflecting their relationship. According to the slope A and intercept B of
 421 that regression line, the correlations between the reference wind field and model prediction can be
 422 well examined, where the ideal values of A and B are 1 and 0, respectively.

423 Secondly, a similar approach to Vollmer et al. [19] is adopted to sample the wake flow data at
 424 different downwind locations in the superposed wake area, using virtual wind turbines of the same
 425 type as in the numerical simulations. The difference from Vollmer et al. [19] is that the method is no
 426 longer used to identify the wake center, but focuses on predicting the power generation of the
 427 hypothetical wind turbine at the given downwind location. The virtual turbine rotors are arranged
 428 as shown in Figure 6. For different test cases, they sweep across the wake area behind the second or
 429 third wind turbine, which makes it possible to calculate the continuous change in power output of
 430 the downwind turbine. In particular, for a virtual wind turbine placed at a given downwind location,
 431 its normalized available power can be obtained by averaging the cubed wind speed over a circular
 432 plane with a diameter of D centered around the turbine hub height, based on the extracted wake flow
 433 data:

$$P_{av}^* = \frac{\int 0.5\rho u_w^3 dA}{\int 0.5\rho u_0^3 dA} \quad (29)$$

434 With the above definition, if there is a real wind turbine in that given location, the normalized
 435 power it generated is equal to P_{av}^* multiplied by the power coefficient C_p . In this way, the ability for
 436 a wide variety of turbine array configurations to extract wind energy can be well quantified,
 437 regardless of whether the downstream turbine experiences full-wake or partial-wake conditions.
 438 Therefore, it is useful for assessing the predictive performance and universality of wind farm wake
 439 models.



440 **Figure 6.** Illustrative sketch of the distribution of virtual turbines used to evaluate the performance of
 441 analytical models. The black solid lines represent the positions of the real wind turbines, and the black
 442 dots denote the locations of the virtual turbines.

443

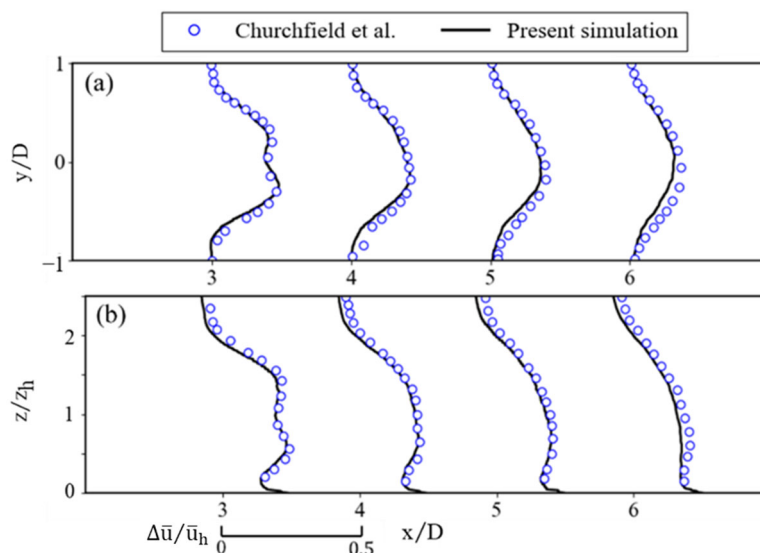
444 **4. Results and discussions**

445 In Section 4.1, the wake characteristics and aerodynamic coefficients for a single wind turbine at
 446 different yaw angles are analyzed, with the purpose of determining the unknown parameters in the
 447 newly proposed model and performing a priori calibration of the performance of the sub-modules.
 448 Then, in Section 4.2, the wake fields obtained from the new proposed model and the conventional
 449 analytical wind farm model are compared against the LES results for different test cases. Additionally,
 450 since the main objective of active yaw control is to maximize the total power production of wind farm,
 451 in Section 4.3, the change in power gain of downstream wind turbines at different yaw angle
 452 distributions are evaluated and discussed.

453 *4.1. single turbine scenario*

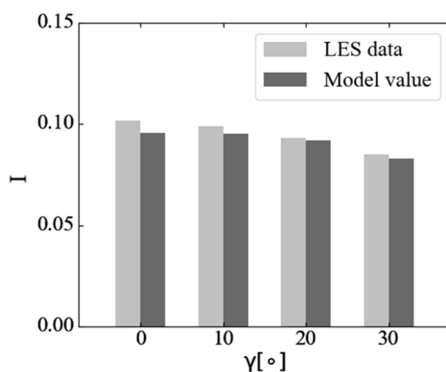
454 Firstly, we examine the accuracy of large eddy simulations conducted by the SOWFA tool. In
 455 Figure 7, the mean streamwise velocity deficit profiles under non-yawed conditions obtained from
 456 the present LES are compared with the result of Churchfield et al.[59], which is widely accepted and
 457 cited. In their works, the wake flow behavior and the aerodynamic performance of the NREL 5-MW
 458 wind turbine were studied under the same inflow condition as the current simulation. As evident in
 459 Figure 7, the LES data in the current simulation agrees well with that from Churchfield et al.

460 Considering that in all numerical experiments in this work, except for the yaw angle distribution
 461 and the number of wind turbines, other settings, such as the computational domain, boundary
 462 conditions, inflow condition, mesh resolution, time step, are all the same. Consequently, according
 463 to the aforementioned comparison for the wake of a single wind turbine at zero-yaw, it is reasonable
 464 to acknowledge that the LES results of the wind turbine wake in the current work are accurate. This
 465 indicates that the LES wind field can be used as a reference to evaluate the analytical model
 466 predictions.



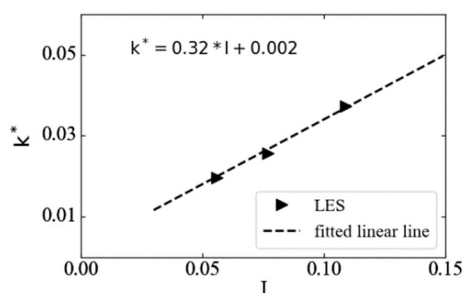
467 **Figure 7.** Profiles of the normalized mean streamwise velocity deficit in (a) the horizontal hub-height
 468 plane and (b) the vertical plane normal to the wind turbine under non-yawed conditions.

469 Next, in Figure 8, the predicted values of I at $x=7D$ downstream of the wind turbine are
 470 compared against those obtained from large eddy simulation (LES). The reason for choosing this
 471 configuration is that, for all test cases with multiple turbines in the current work, the inter-turbine
 472 spacing is fixed at 7 rotor diameters. As apparent in Figure 8, the method of Niayifar et al. [44],
 473 described in detail in Section 2.4, can provide a good prediction of the streamwise turbulence
 474 intensity at different yaw angles.



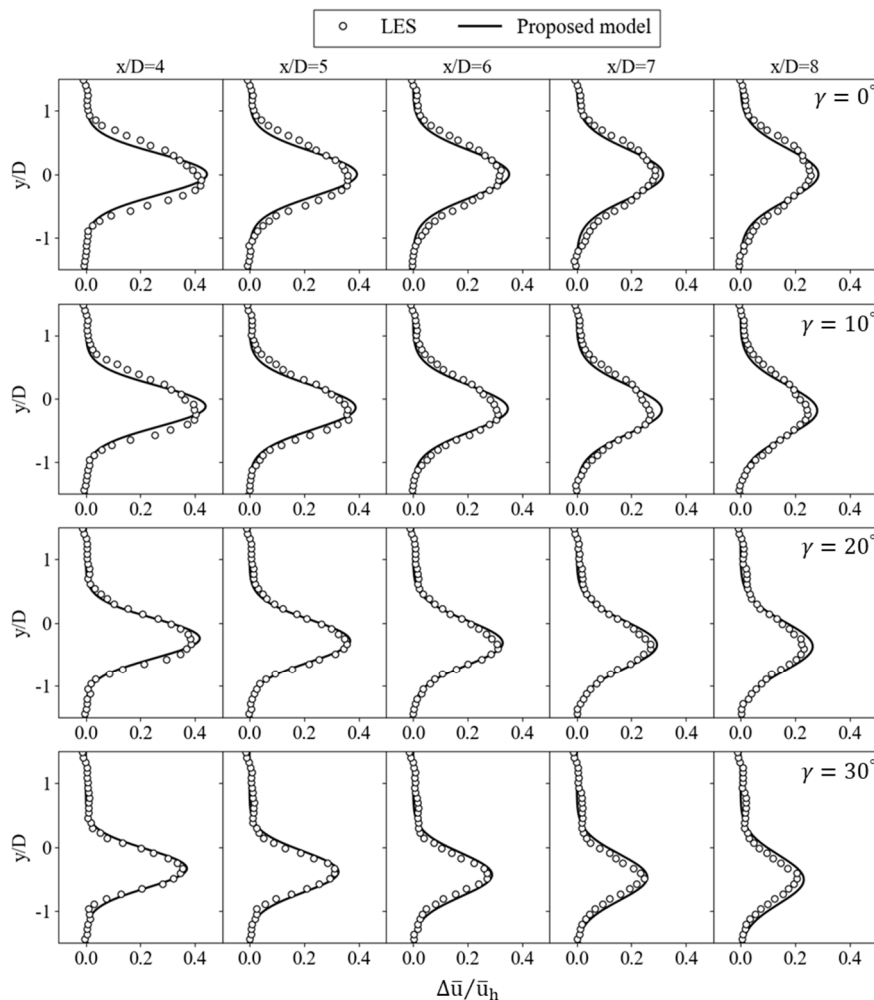
475 **Figure 8.** Values of the local streamwise turbulence intensity at $x = 7D$ behind a single wind turbine
 476 for different yaw angles. The grey bars indicate the LES data and the black bars denote the model
 477 predictions.

478 In Figure 9, the wake width growth rate behind the NREL 5-MW wind turbine is plotted as
 479 a function of the streamwise turbulence intensity at hub height. It is shown that the k^* value
 480 does change approximately linearly with I , as assumed by Equation (21). Additionally, from the
 481 fitted line of the simulated data, k_a and k_b in Equation (21) are determined to be 0.32 and 0.002,
 482 respectively.



483 **Figure 9.** Variations in wake width growth rate for the NREL 5-MW wind turbine with the streamwise
 484 turbulence intensities at hub height.

485 To calibrate the settings of k_a and k_b , here we compare the LES results for a single wind turbine
 486 at different yaw angles to the predictions of the new proposed model (note that, since only a single
 487 turbine is considered, the new model is equivalent to the single wake model derived by Wei et al.[32]).
 488 In particular, with $k_a = 0.32$, $k_b = 0.002$ and $I = 0.056$, the wake width growth rate for the wind turbine
 489 is $k^* = 0.02$, which is around the same as the suggested value in Ref.[32]. Figure 10 presents lateral
 490 profiles of the normalized mean streamwise velocity deficit at different downwind locations.
 491 Obviously, good consistency is found between the proposed model predictions and the LES data for
 492 different yaw angles, indicating that the current settings of k_a and k_b are reasonable. This also lays
 493 the foundation for further applying the new proposed model to simulate multiple wind turbine
 494 wakes under yawed conditions.

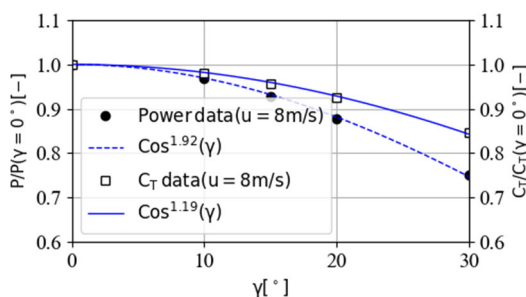


495
496
497

Figure 10. Lateral profiles of the normalized streamwise velocity deficit in the wake of a turbine with $\gamma=0^\circ, 10^\circ, 20^\circ$ and 30° : LES data (open circle) and new proposed model (black solid line)

498
499
500
501
502
503
504

What's more, as illustrated in Section 2.5, to give the aerodynamic performance of a wind turbine under yaw misalignment conditions, the cosine exponents p and q in Equations (27) and (28) should be determined. Following the approach of Dahlberg et al. [57], we in Figure 11 plot the power and thrust coefficients of the NREL 5-MW wind turbine at different yaw angles, and normalized them by their maximum values at $\gamma = 0^\circ$, respectively. It can be seen that in our numerical simulations, the normalized power production approximately varies as $\cos^{1.92}\gamma$, and C_T versus γ has a shape similar to $\cos^{1.19}\gamma$.



505
506
507

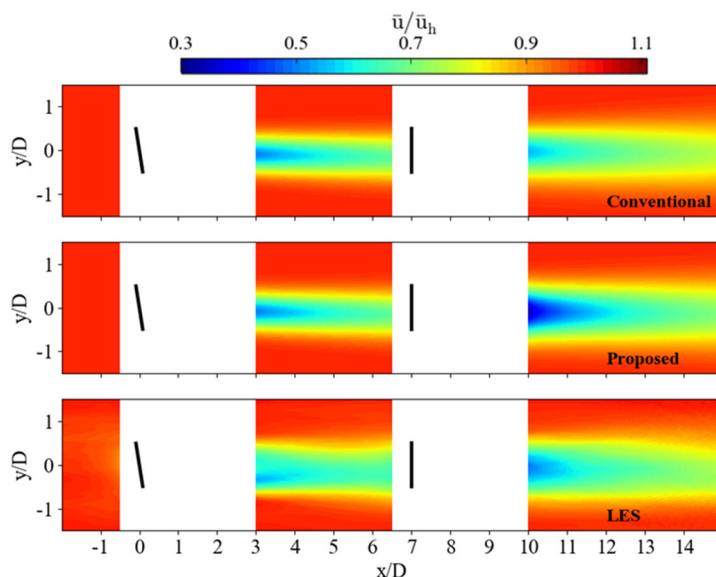
Figure 11. Changes in the normalized power production and thrust coefficient of the NREL 5-MW wind turbine for different yaw angles. Black circles/squares correspond to the simulated data and the blue solid/dashed line represent Cosine fits.

508
509

4.2. multiple-turbine wake analysis

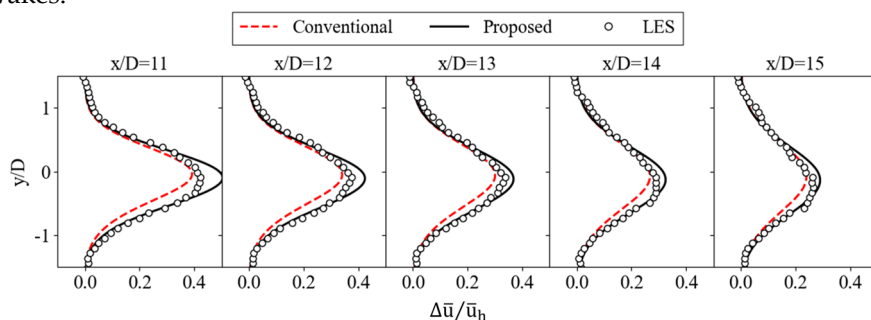
4.2.1 Test case 1(two aligned wind turbines with the front one being yawed 10°)

510 The two-turbine array displayed in Figure 12 is the first test case, in which the front wind turbine
 511 yaws by 10° . As presented, when the first turbine operates with a small yaw angle, the wake width
 512 and streamwise velocity deficit in the overlapped wake are under-predicted by the conventional
 513 analytical model. Oppositely, an over-estimated velocity deficit is shown in the predictions of the
 514 new model, especially in the near-wake. However, as the wake going downstream, the new proposed
 515 model predictions gradually converge to the LES data, and in a whole, compared to the conventional
 516 model, the new proposed model provides a better prediction result.



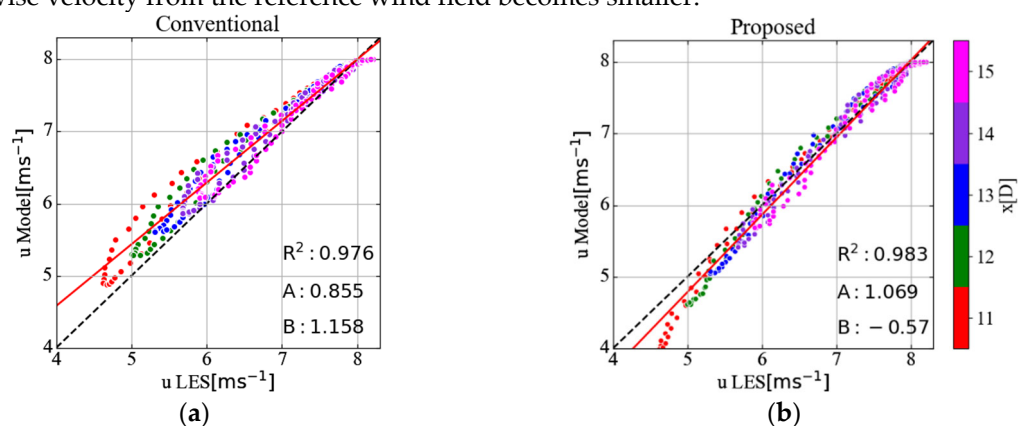
517 **Figure 12.** Contours of the normalized streamwise velocity in the horizontal hub-height plane for two
 518 aligned wind turbines when the front turbine is yawed 10° : Conventional analytical model(top), new
 519 proposed model (middle) and the large-eddy simulations (bottom).

520 To further evaluate the difference between the LES flow field and the model predictions, we in
 521 Figure 13 compare the lateral profiles of the normalized streamwise velocity deficit behind the second
 522 wind turbine, at the chosen downwind locations ($x=11D, 12D, 13D, 14D, 15D$). Similar to the above
 523 analysis, the conventional model using the sum of squares superposition method is found to
 524 underestimate the velocity deficit, and more seriously, it fails to capture the "secondary wake
 525 steering". For the newly proposed model, it exhibits some biases towards overestimating the velocity
 526 deficit with respect to the reference wind field, obvious before $x/D=12$, but as the wake develops
 527 further downstream, the situation is greatly improved. The above departure occurs in the physical-
 528 based new model may be attributed to the limitation of the single wake model[19] used, which is
 529 developed for far wake modeling and some assumptions it adopted are only applicable to the fully
 530 developed wakes.



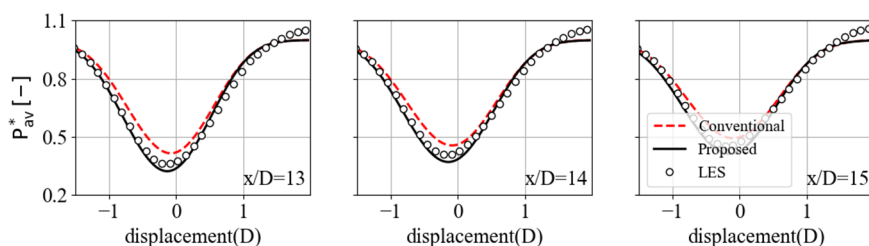
531 **Figure 13.** Lateral profiles of the normalized streamwise velocity deficit in the wakes at different
 532 downwind locations behind the second turbine when the front turbine is yawed 10° : LES data (open
 533 circle), new proposed model (black solid line), and conventional analytical model (red dashed line).

534 What's more, we also perform regression analysis on the streamwise velocity at different cross-
 535 sections, and the results is shown in Figure 14. The x-axis and y-axis in the plot represent the
 536 streamwise wake velocity extracted from the large eddy simulation and predicted by the analytical
 537 model, respectively. The black diagonal line indicates the two are equal to each other. As mentioned
 538 above, compared with the reference wind field, the predictions of both analytical models have large
 539 errors in the combined wake near the second wind turbine, especially in the wake center region. The
 540 distinguish is that the velocity deficit is overestimated by the new model while it is under-predicted
 541 by the conventional model. As such, the intercept of the regression line is large for both models.
 542 However, in contrast, the absolute value of the intercept for the new model is only about half of that
 543 for the conventional model, indicating that the new model performs a little better. Additionally, one
 544 can also observed that, the slope of the regression line for the new proposed model is also relatively
 545 closer to the ideal value, this is due to the fact that the new model can reasonably predict the wake
 546 deflection in the overlapped wake, and at further downstream positions, the deviation of its predicted
 547 streamwise velocity from the reference wind field becomes smaller.



548 **Figure 14.** Scatter plot and corresponding regression line of the streamwise wake velocity as predicted
 549 using (a) the conventional analytical model and (b) the new proposed model, in relation to the
 550 reference wind field calculated with large-eddy simulations (LESs).

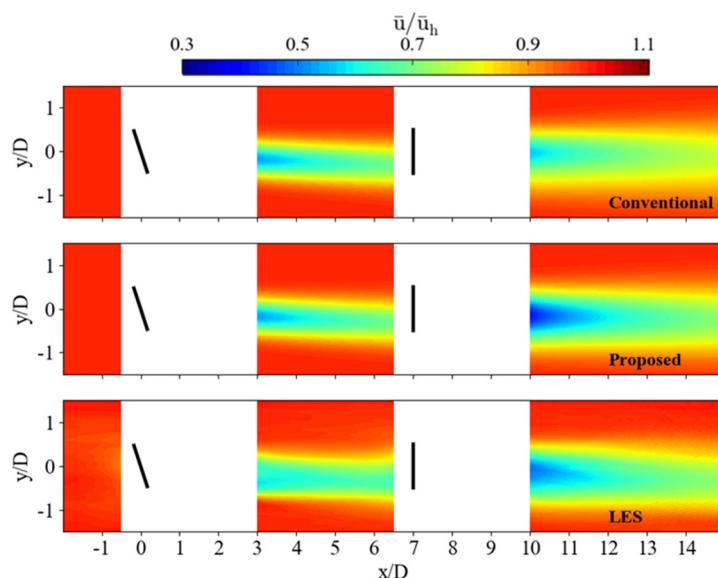
551 Since the main interest for implementing active yaw control is to seek optimal power production
 552 of the entire wind farm, accurately predict the power output of wind turbines is important for
 553 analytical wake models. As shown in Figure 15, the normalized available power of virtual wind
 554 turbines located behind the second turbine are computed, sweeping the spanwise direction of the
 555 wake flow at several downwind locations. It is apparent that there is a substantial difference between
 556 the conventional model predictions and the LES data. To be specific, in LES, the "profile" of power
 557 deficit is further deflected with respect to the incoming steered wake. However, the conventional
 558 model shows that the power deficit "profile" only shifts slightly as the wake traveling downstream,
 559 this is because no effect of the transverse velocity induced by upstream yawed turbine is considered.
 560 On the contrary, the new proposed model agrees well with the LES data except at the edge of the
 561 wake, demonstrating the potential of applying it to predict the wake steering performance.



562 **Figure 15.** Power production of a hypothetical turbine behind the second turbine when the front
 563 turbine is yawed 10° : LES data (open circle), new proposed model (black solid line), and conventional
 564 analytical model (red dashed line).

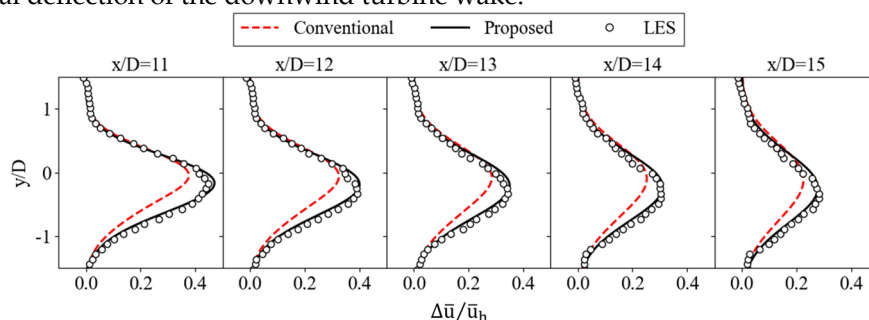
565 4.2.2 Test case 2(two aligned wind turbines with the front one being yawed 20°)

566 Next, take a look at another two-turbine array with the upstream turbine being yawed 20°. Figure
 567 16 shows the contours of the normalized streamwise velocity in the horizontal plane at hub height.
 568 As seen in the SOWFA case, due to a larger yaw angle of the front wind turbine, the "secondary wake
 569 steering" phenomenon in the overlapped wake becomes more obvious. In addition, some disparities
 570 occur between the LES results and the conventional model, which cannot predict the continuous
 571 deflection of the wake behind the second wind turbine. In contrast, the newly proposed model well
 572 captures the flow characteristics of the combined wake.



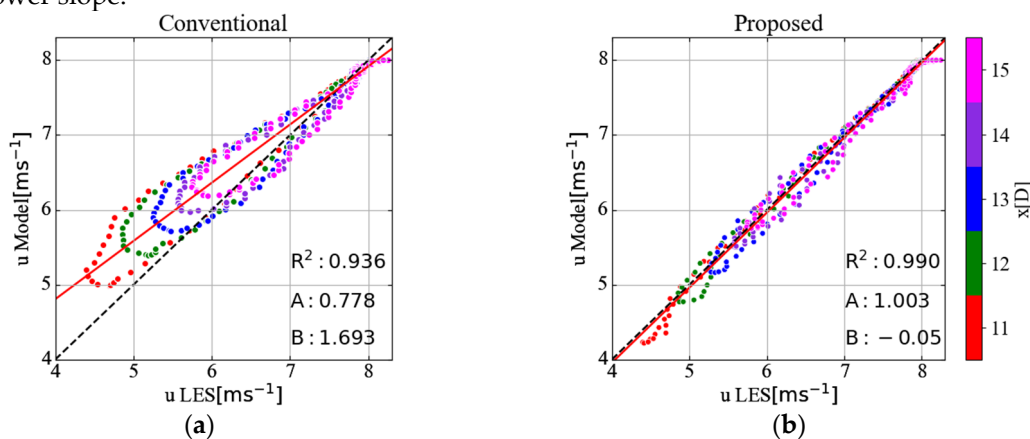
573 **Figure 16.** Contours of the normalized streamwise velocity in the horizontal hub-height plane for two
 574 aligned wind turbines when the front turbine is yawed 20°: Conventional analytical model(top), new
 575 proposed model (middle) and the large-eddy simulations (bottom).

576 Figure 17 presents the development of the horizontal profiles of the normalized streamwise
 577 velocity deficit at different downwind distances. As shown in the SOWFA case, with increasing yaw
 578 angle of the front wind turbine, the second turbine's wake appears to deflect larger, which is
 579 consistent with the above analysis. What's more, good agreement is found between the LES data and
 580 the predictions of the new model. As for the conventional analytical model, it underestimates the
 581 velocity deficit in the superposed wake area, and does not capture the "secondary wake steering"
 582 phenomenon. This is because in the conventional model, the impact of the front turbine wake on the
 583 downstream wind turbines mainly includes reduced velocity and increased turbulence intensity
 584 (reflected by the change in wake width growth rate). Obviously, neither of these two effects can cause
 585 the additional deflection of the downwind turbine wake.



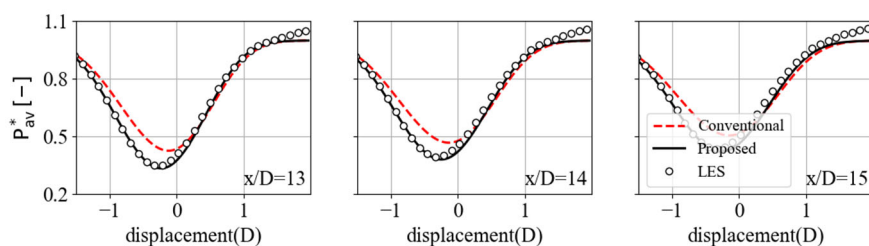
586 **Figure 17.** Lateral profiles of the normalized streamwise velocity deficit in the wakes at different
 587 downwind locations behind the second turbine when the front turbine is yawed 20°: LES data (open
 588 circle), new proposed model (black solid line), and conventional analytical model (red dashed line).

589 The results of the regression analysis for Test case 2 are collected in Figure 18. According to the
 590 slope A and the intercept B, we can see that the new analytical model is close to a perfect regression
 591 line. However, these terms in the conventional model don't show good results, which can be
 592 explained as follows: At each selected downwind position, the maximum velocity deficit in the wake
 593 center region is under-estimated, as presented in Figure 17; In addition, the conventional model
 594 cannot capture the "secondary wake steering" effect, so the deviation between its predictions from
 595 the reference wind field becomes more larger as the wake moving sideways, especially in the wake
 596 steering direction. Consequently, the regression line for the conventional model has a higher intercept
 597 and a lower slope.



598 **Figure 18.** Scatter plot and corresponding regression line of the streamwise wake velocity as predicted
 599 using (a) the conventional analytical model and (b) the new proposed model, in relation to the
 600 reference wind field calculated with large-eddy simulations (LESs).

601 To further explore the difference in wake predictions by the two analytical models, power
 602 outputs of virtual turbines are calculated, and the results are displayed in Figure 19. Apparently, the
 603 new proposed model shows better performance than the conventional model by closely following
 604 the power profile of the reference case. What's more, as expected, due to the failure to capture the
 605 "secondary steering" effect, the substantial change of the power output for wind turbine running in
 606 the combined wake is much different from the conventional model prediction. This again supports
 607 the notion that when considering an array of more than two turbines operating in yawed conditions,
 608 the effect of vortex interactions must be taken into account.
 609

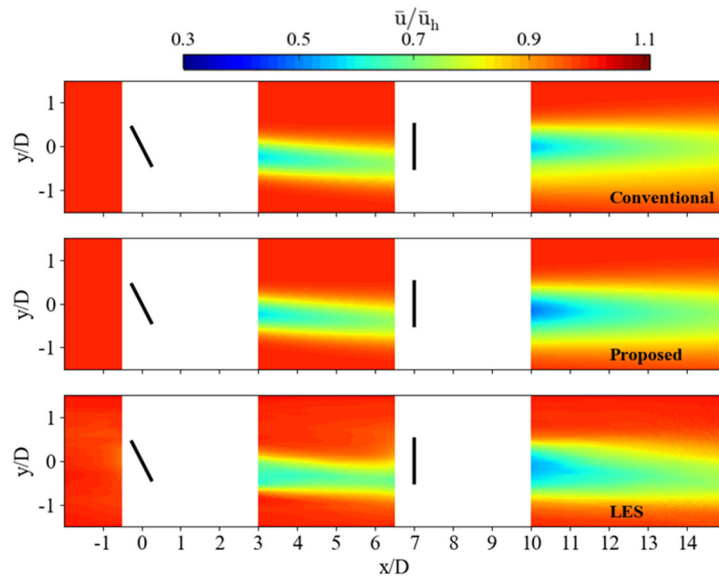


610 **Figure 19.** Power production of a hypothetical turbine behind the second turbine when the front
 611 turbine is yawed 20°: LES data (open circle), new proposed model (black solid line), and conventional
 612 analytical model (red dashed line).

613 4.2.3 Test case 3 (two aligned wind turbines with the front one being yawed 30°)

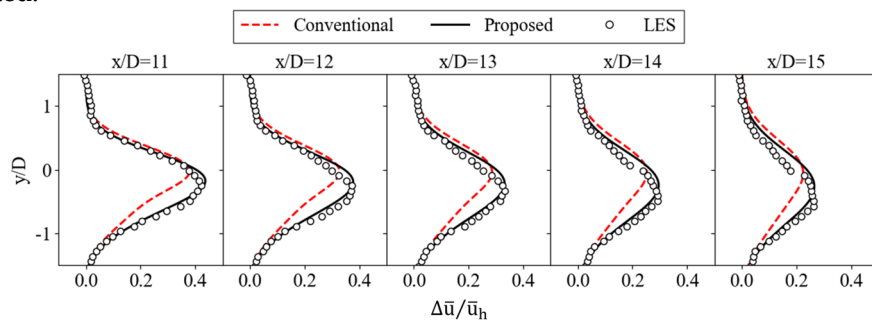
614 In here, the contour plot of turbine wake in the third case are presented, which is a two-turbine
 615 scenario where the front turbine is yawed by 30°. As shown in Figure 20, for the wake flow
 616 downstream of the second turbine, continuous wake deflection is observed in SOWFA case, which is
 617 in line with previous analysis. Additionally, the prediction of the new model is found to be in good
 618 agreement with the LES results, it can well capture the steered wake in the superposed area. However,

619 in the conventional analytical model, since the influence of the persistent transverse velocity induced
 620 by the front yawed turbine is not considered, the prediction result greatly deviates from the reference
 621 case.



622 **Figure 20.** Contours of the normalized streamwise velocity in the horizontal hub-height plane for two
 623 aligned wind turbines when the front turbine is yawed 30°: Conventional analytical model(top), new
 624 proposed model (middle) and the large-eddy simulations (bottom).

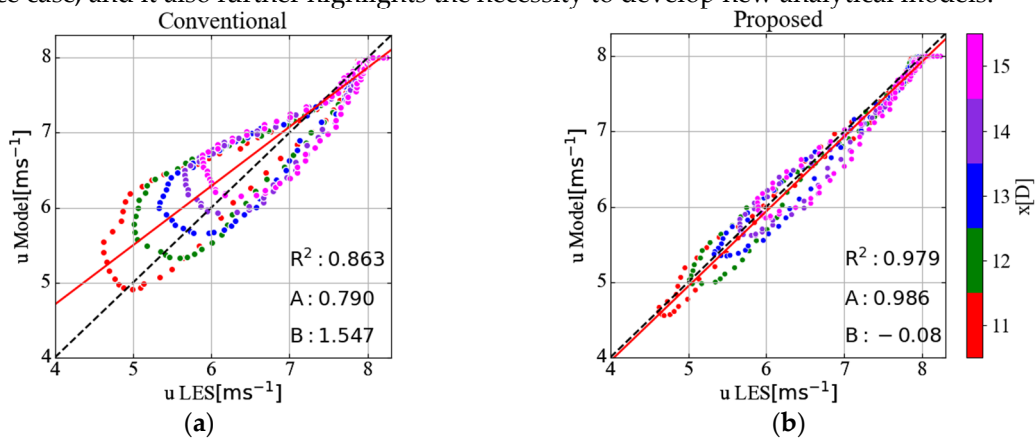
625 Figure 21 presents the detailed lateral distribution of the velocity deficit at different downwind
 626 locations. As seen, the new proposed model agrees well with the LES data, showing the ability to
 627 capture the distribution characteristics of the streamwise wake . While for the conventional model, it
 628 fails to predict the wake deflection in the superposed area, and further, quite different from the
 629 reference wind field. To be specific, the velocity deficit in the lower half of the combined wake
 630 predicted by the conventional model is seriously under-estimated while the upper part is slightly
 631 over-estimated.



632 **Figure 21.** Lateral profiles of the normalized streamwise velocity deficit in the wakes at different
 633 downwind locations behind the second turbine when the front turbine is yawed 30°: LES data (open
 634 circle), new proposed model (black solid line), and conventional analytical model (red dashed line).

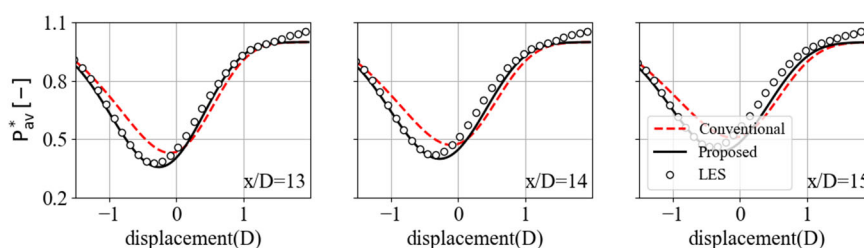
635 As evident in Figure 22, the regression analysis for Test Case 3 almost reproduces the results of
 636 Test Case 2, with the difference that, for the newly proposed model, the regression line is no longer
 637 so close to perfection; while for the conventional model, the deviation of the slope and intercept of
 638 the regression line from their ideal values becomes smaller. This outcome can be explained as follows:
 639 Different to the almost thoroughly underestimated velocity deficit in Test case 2, in Test Case 3
 640 considered here, although the streamwise velocity deficit predicted by the conventional model is also
 641 lower than the LES data in the wake steering direction, it is slightly overestimated in another half
 642 part of the combined wake. It is the uneven distribution that leads to a relatively higher slope and a

643 lower intercept for the conventional model. Another striking observation in Figure 22 is the
 644 determination coefficient for the conventional model, whose value is the lowest among all the test
 645 cases of the two-turbine array, indicating a poor correlation between the model prediction and the
 646 reference case, and it also further highlights the necessity to develop new analytical models.



647 **Figure 22.** Scatter plot and corresponding regression line of the streamwise wake velocity as predicted
 648 using (a) the conventional analytical model and (b) the new proposed model, in relation to the
 649 reference wind field calculated with large-eddy simulations (LESs).

650 Figure 23 displays the power output for virtual wind turbines located in the superposed wake
 651 area, it can be observed that, the new analytical wind farm model provides a better prediction
 652 compared to the conventional one, but its result is less accurate on the right side, which may be
 653 related to the follow factors: For the single wake model adopted in the present work, the lateral
 654 velocity profile at hub height is assumed to have a symmetric Gaussian shape in the far wake.
 655 However, as indicated by previous experimental results [21], the wake profiles are slightly skewed
 656 by the strong transverse velocity distribution, especially for larger yaw angles. Furthermore, the
 657 partial-wake conditions experienced by the second wind turbine may be another contributor, it can
 658 give rise to an uneven wake recovery rate between the two sides of the wake. Consequently, in the
 659 right part of the power deficit "profile" in Figure 23, the new model shows a little deviation from the
 660 reference.

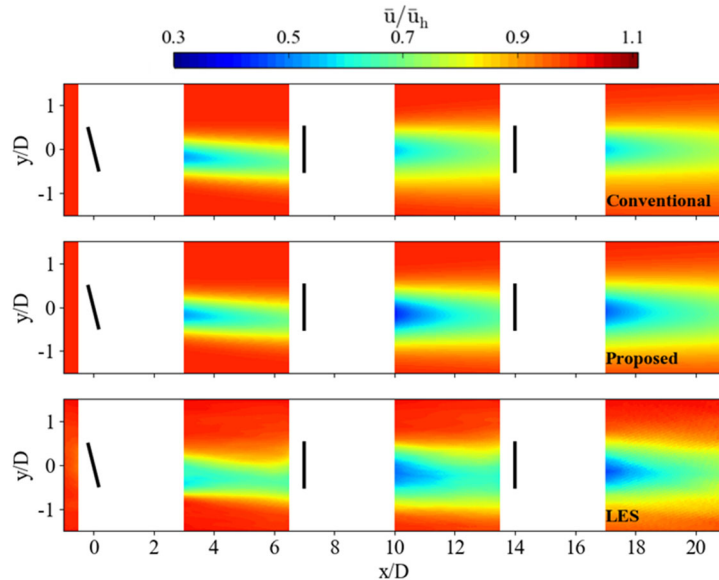


661 **Figure 23.** Power production of a hypothetical turbine behind the second turbine when the front
 662 turbine is yawed 30°: LES data (open circle), new proposed model (black solid line), and conventional
 663 analytical model (red dashed line).

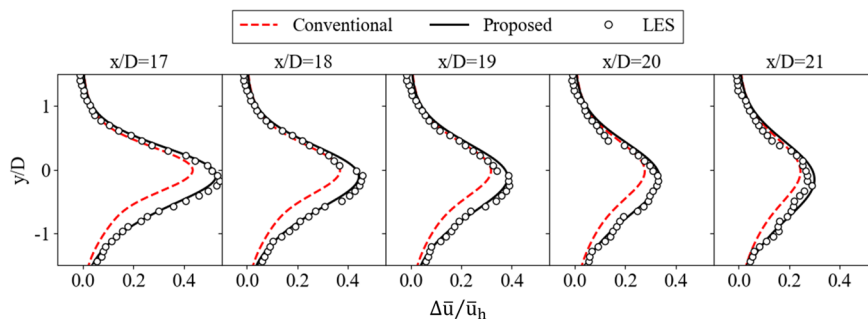
664 4.2.4 Test case 4(three aligned wind turbines with the front one being yawed 20°)

665 In order to further investigate the "secondary wake steering" effect on wake evolution and
 666 evaluate the performance of analytical wake models, a three-turbine array simulation is performed,
 667 where the first wind turbine is yawed 20° and the other two turbines are maintained non-yawed. As
 668 apparent in Figures 24 and 25, the new proposed model is shown to be able to accurately predict
 669 deflections up to the third turbine's wake, consistent with the LES data. However, the conventional
 670 model based on sum of squares superposition method cannot capture such wake behavior. On the

671 one hand, this result indicates that the transverse velocity in upstream yawed turbine wakes, induced
 672 by the CPV, can persist past downwind turbines, even throughout the whole wind farm. Therefore,
 673 it is necessary to take its effects into wake model development and wake-redirection control design.
 674 On the other hand, the newly proposed model demonstrates its improvements in predicting for more
 675 than two turbines in a row under yawed conditions, addresses the concern about its universality, and
 676 also lays a foundation for its further application in the real-world engineering scenarios.



677 **Figure 24.** Contours of the normalized streamwise velocity in the horizontal hub-height plane for
 678 three aligned wind turbines when the front turbine is yawed 20°: Conventional analytical model(top),
 679 new proposed model (middle) and the large-eddy simulations (bottom).

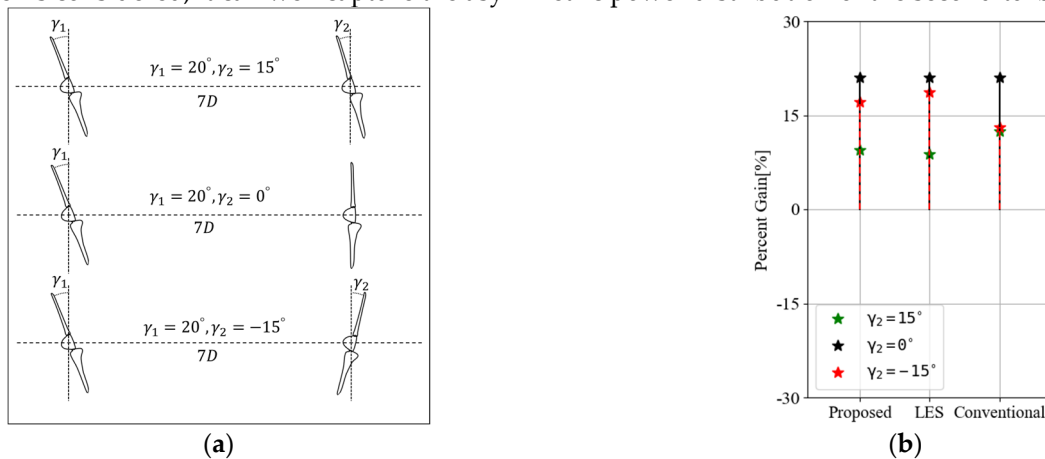


680 **Figure 25.** Lateral profiles of the normalized streamwise velocity deficit in the wakes at different
 681 downwind locations behind the third turbine when the front turbine is yawed 20°: LES data (open
 682 circle), new proposed model (black solid line), and conventional analytical model (red dashed line).

683 4.3. power output comparison

684 In this section, for assessing the predictive performance of analytical models on power output,
 685 simulations on another several two-turbine arrays are carried out. Panel (a) in Figure 26 shows the
 686 schematic diagram of yaw angle combinations, in which, the front wind turbine is always yawed
 687 20°, while the second turbine is operating with different yaw misalignments: 15°(top row), 0°(middle
 688 row) and -15°(bottom row). With the same numerical settings of the test cases in Section 4.2, for the
 689 two-turbine array considered here, the inlet wind speed is 8 m/s and streamwise turbulence intensity
 690 at hub height is around 5.6% , and the separation between turbines is fixed at 7 times rotor diameter
 691 in the streamwise direction. Note that since the second wind turbine runs in a single yawed wake
 692 instead of a combined wake, the "secondary wake steering" effect has no impact on its power
 693 generation. In other words, the new proposed model for these cases is equivalent to only the "added
 694 yaw angle" effect addressed in Section 2.3.

695 Figure 26(b) shows the relative power gains for the second wind turbine in each yaw angle
 696 distribution relative to a baseline case of all turbines aligned. As apparent in the plot, in the
 697 conventional model predictions, the positive or negative yaw of the second turbine seems to have
 698 little effect on its power production. However, from the LES data, this is not the case. In particular,
 699 when the second turbine yaws towards the same direction as the first one, its power output is less
 700 than that when they yaw in opposite directions. This can be explained by the "added yaw angle".
 701 According to Equations (19) and (20), when the yaw direction of the two turbines is the same, the real
 702 yaw angle of the downstream wind turbine is greater than its set value, causing a decrease in its
 703 power generation, and vice versa. For the newly proposed model, since the effect of the "added yaw
 704 angle" is considered, it can well capture the asymmetric power distribution of the second turbine.



705 **Figure 26.** (a) Schematic diagram of the yaw angle distributions for two-turbine cases where the front
 706 turbine is yawed 20° and the second turbine is yawed 15° (top row), 0° (middle row), and -15°
 707 (bottom row). (b) Percent change of power production for the second turbine in each yaw angle distribution.

708 5. Conclusions

709 Recent studies have emphasized the importance of counter-rotating vortices in wake steering,
 710 these large-scale structures not only deform the wake of a yawed wind turbine, but also can make
 711 the wake trajectory of a non-yawed downwind turbine deviates from its rotor centerline, called
 712 "secondary wake steering" phenomenon. Due to these vortices can propagate a long distance, and
 713 thus, impact the wake steering performance of larger turbine arrays, it is necessary to include the
 714 effects of counter-rotating vortices in analytical wake model development and wind farm controller
 715 design. However, in the common analytical models for active yaw control, only the streamwise
 716 velocity from each individual wind turbine is calculated, without considering the transverse velocity
 717 induced by the vortex structures, this omission may lead to errors in model predictions. In order to
 718 compensate for it, a new analytical wind farm model is proposed, in which, a physical-based
 719 momentum-conserving wake superposition method [37] is adopted to model the interaction of
 720 multiple wakes; and in the application, not only the streamwise velocity is combined, but also the
 721 transverse velocity, which makes it possible to reproduce the secondary wake steering effect crucial
 722 to active yaw control. What's more, an "added yaw angle" is defined for a downwind turbine
 723 operating in upstream yawed turbine wakes, to reflect the change in local wind direction it perceives.
 724 Then, the total yaw angle including the defined "added yaw angle", instead of the set value of the
 725 yaw angle, is used as an input parameter for the single wake model derived by Wei and Wan[32] to
 726 calculate the individual wake.

727 For validation purposes, lots of numerical simulations are conducted using the SOWFA tool, and
 728 the obtained LES wind field is used as a reference to assess the analytical model performance.
 729 Detailed comparisons show that, the newly proposed model agrees well with LES results and
 730 outperforms the representative conventional analytical model in almost all test cases. In particular,
 731 the new model gives an accurate prediction on the wake velocity distribution in the superposed area,
 732 and can successfully reproduce the "secondary wake steering" phenomenon. By contrast, the

733 conventional model does not perform as such well, it tends to underestimate the total velocity deficit,
 734 and more importantly, the prediction results not support the aforementioned "secondary wake
 735 steering". The departure is largely because the sum of squares operation adopted to combine the
 736 wakes is an empirical formula without solid physical foundation, and no effects of the vortex
 737 interactions is considered. What's more, since the "added yaw angle" effect caused by the upstream
 738 transverse velocity is taken into account in the new model, it shows an ability to accurately predict
 739 the power gain of wake-affected downstream wind turbines.

740 In future studies, we will further evaluate the performance of the newly proposed analytical
 741 model in predicting deep turbine array (i.e., cases with several rows of wind turbines). Moreover,
 742 due to the merits of low computational cost and high accuracy, the new model will be used as a tool
 743 to explore the potential of active yaw control in wind farm power optimization.
 744

745 **Author Contributions:** The paper was a collaborative effort among the authors. Dezhi Wei performed the
 746 modeling, designed the structure, and wrote the paper. Decheng Wan supervised the related work and polished
 747 the language of the paper.

748 **Acknowledgments:** This work was supported by National Natural Science Foundation of China (Grant No.
 749 52131102, 51879159), National Key Research and Development Program of China (2019YFB1704200 and
 750 2019YFC0312400), to which the authors are most grateful.

751 **Conflicts of Interest:** The authors declare no conflict of interest.

752 References

- 753 1. Gaumont, M.; Réthoré, P.E.; Ott, S.; Peña, A.; Bechmann, A.; Hansen, K.S. Evaluation of the wind direction
 754 uncertainty and its impact on wake modeling at the Horns Rev offshore wind farm. *Wind Energy* **2014**, *17*,
 755 1169–1178.
- 756 2. Adaramola M.S.; Krogstad P.Å. Experimental investigation of wake effects on wind turbine performance.
 757 *Renew. Energy* **2011**, *36*, 2078–2086.
- 758 3. Dilip, D.; Porté-Agel, F. Wind turbine wake mitigation through blade pitch offset. *Energies* **2017**, *10*, 757.
- 759 4. Lee, J.; Son, E.; Hwang, B.; Lee, S. Blade pitch angle control for aerodynamic performance optimization of
 760 a wind farm. *Renew. Energy* **2013**, *54*, 124–130.
- 761 5. Fleming, P.A.; Gebraad, P.M.O.; Lee, S.; van Wingerden, J.W.; Johnson, K.; Churchfield, M.; Michalakes, J.;
 762 Spalart, P.; Moriarty, P. Evaluating techniques for redirecting turbine wakes using SOWFA. *Renew. Energy*
 763 **2014**, *70*, 211–218.
- 764 6. Bartl, J. M. S.; Muhle, F. V.; Sætran, L. R. Wind tunnel study on power output and yaw moments for two
 765 yaw-controlled model wind turbines. *Wind Energ. Sci.* **2018**, *3*, 489.
- 766 7. Campo, V.; Ragni, D.; Micalef, D.; Diez, F.J.; Simão-Ferreira, C.J. Estimation of loads on a horizontal axis
 767 wind turbine operating in yawed flow conditions. *Wind Energy* **2015**, *18*(11), 1875–1891.
- 768 8. Bastankhah, M.; Porté-Agel, F. A wind-tunnel investigation of wind-turbine wakes in yawed conditions. *J.*
 769 *Phys. Conf. Ser.* **2015**, *625*, 012014.
- 770 9. Zong H, Porté-Agel, F. Experimental investigation and analytical modelling of active yaw control for wind
 771 farm power optimization. *Renew. Energy* **2021**, *170*, 1228–1244.
- 772 10. Howland MF, Lele SK, Dabiri JO. Wind farm power optimization through wake steering. *Proc Natl Acad*
 773 *Sci* **2019**, *116*(29), 14495–14500.
- 774 11. Lee, H.; Lee, D. Wake impact on aerodynamic characteristics of horizontal axis wind turbine under yawed
 775 flow conditions. *Renew. Energy* **2019**, *136*, 383–392.
- 776 12. van Dijk, M.; van Wingerden, J.W., Ashuri, T., Li, Y. Wind farm multi-objective wake redirection for
 777 optimizing power production and loads. *Energy* **2017**, *121*, 561–569.
- 778 13. Bartl, Jan.; Mühle, F.; Sætran, L. Wind tunnel study on power output and yaw moments for two yaw-
 779 controlled model wind turbines. *Wind Energ. Sci.* **2018**, *3*, 489–502.
- 780 14. Krogstad, P.; Adaramola, M.S. Performance and near wake measurements of a model horizontal axis wind
 781 turbine. *Wind Energy* **2012**, *15*, 743–756.
- 782 15. Ozbay, A.; Tian, W.; Yang, Z.; Hu, H. Interference of wind turbines with different yaw angles of the
 783 upstream wind turbine. In Proceedings of the 42nd AIAA Fluid Dynamics Conference and Exhibit, New
 784 Orleans, LA, USA, 25–28 June 2012; p. 2719.

- 785 16. Bastankhah, M.; Porte-Agel, F. Wind tunnel study of the wind turbine interaction with a boundary-layer
786 flow: Upwind region, turbine performance, and wake region. *Phys. Fluids* **2017**, *29*, 065105.
- 787 17. Jiménez, Á.; Crespo, A.; Migoya, E. Application of a LES technique to characterize the wake deflection of a
788 wind turbine in yaw. *Wind Energy* **2010**, *13*, 559–572.
- 789 18. Bartl, J.; Muhle, F.; Schottler, J.; Sætran, L.; Peinke, J.; Adaramola, M.; et al. Wind tunnel experiments on
790 wind turbine wakes in yaw: Effects of inflow turbulence and shear. *Wind Energ. Sci.* **2018**, *3*, 329–343.
- 791 19. Vollmer, L.; Steinfeld, G.; Heinemann, D.; Kühn, M. Estimating the wake deflection downstream of a wind
792 turbine in different atmospheric stabilities: An LES study. *Wind Energ. Sci.* **2016**, *1*, 129–141.
- 793 20. Howland, M.F.; Bossuyt, J.; Martínez-Tossas, L.A.; Meyers, J.; Meneveau, C. Wake structure in actuator
794 disk models of wind turbines in yaw under uniform inflow conditions. *J. Renew. Sustain. Ener.* **2016**, *8*,
795 043301.
- 796 21. Bastankhah, M.; Porté-Agel, F. Experimental and theoretical study of wind turbine wakes in yawed
797 conditions. *J. Fluid Mech.* **2016**, *806*, 506–541.
- 798 22. Fleming, P.; Annoni, J.; Churchfield, M.; Martinez-Tossas, L.A.; Gruchalla, K.; Lawson, M.; et al. A
799 simulation study demonstrating the importance of large-scale trailing vortices in wake steering. *Wind Energ.*
800 *Sci.* **2018**, *3*, 243–255.
- 801 23. Bay, C.; King, J.; Fleming, P.; Mudafort, R.; Martinez, L. *Unlocking the full potential of wake steering:*
802 *implementation and assessment of a controls-oriented model*; Technical Report; National Renewable Energy Lab.
803 (NREL): Golden, CO(United States), 2019.
- 804 24. Bastankhah, M.; Porté-Agel, F. Wind farm power optimization via yaw angle control: A wind tunnel study.
805 *J. Renew. Sustain. Ener.* **2019**, *11*, 023301.
- 806 25. Gebraad, P., Teeuwisse, F., Wingerden, J., Fleming, P.A., Ruben, S., Marden, J., et al. Wind plant power
807 optimization through yaw control using a parametric model for wake effects – a CFD simulation study.
808 *Wind Energy* **2016**, *19*, 95–114.
- 809 26. Jensen, N. *A note on wind turbine interaction*; Technical report; Ris-M-2411 Risø National Laboratory:
810 Roskilde, Denmark, 1983.
- 811 27. Lin M.; Porté-Agel, F. Large-Eddy Simulation of yawed wind-turbine wakes: comparisons with wind
812 tunnel measurements and analytical wake models. *Energies* **2019**, *12*, 4574.
- 813 28. Xie, S.; Archer, C. Self-similarity and turbulence characteristics of wind turbine wakes via large-eddy
814 simulation. *Wind Energy* **2015**, *18*, 1815–1838.
- 815 29. Chamorro, L.; Porté-Agel, F. A wind-tunnel investigation of wind-turbine wakes: Boundary-layer
816 turbulence effects. *Bound.-Layer Meteorol.* **2009**, *132*, 129–149.
- 817 30. Dou B, Guala M, Lei L, Zeng P. Wake model for horizontal-axis wind and hydrokinetic turbines in yawed
818 conditions. *Appl. Energ.* **2019**, *242*, 1383–1395.
- 819 31. Qian, G.W.; Ishihara, T. A new analytical wake model for yawed wind turbines. *Energies* **2018**, *11*, 665.
- 820 32. Wei, D.Z, Wang, N.N, Wan, D.C. Modeling yawed wind turbine wakes: Extension of a Gaussian-based wake model.
821 *Energies* **2021**, *14*(15), 4494.
- 822 33. Katic, I.; Højstrup, J.; Jensen, N.O. A simple model for cluster efficiency. In Proceedings of the European
823 Wind Energy Association Conference & Exhibition, Rome, Italy, 7–9 October 1986; pp. 407–410.
- 824 34. Shao, Z.Z.; Wu, Y.; Li, L.; Han, S.; Liu, Y.Q. Multiple wind turbine wakes modeling considering the faster
825 wake recovery in overlapped wakes. *Energies* **2019**, *12*, 680.
- 826 35. Crespo, A., Hernández, J., Frandsen, S. Survey of modelling methods for wind turbine wakes and wind
827 farms. *Wind Energy* **1999**, *2*, 1–24.
- 828 36. Martínez-Tossas, L.A.; Annoni, J.; Fleming, P.A.; Churchfield, M.J. The aerodynamics of the curled wake:
829 A simplified model in view of flow control. *Wind Energ. Sci.* **2019**, *4*, 127–138.
- 830 37. Zong, H.H.; Porté-Agel, F. A momentum-conserving wake superposition method for wind farm power
831 prediction. *J. Fluid Mech.* **2020**, *889*, A8.
- 832 38. Coleman, R.P.; Feingold, A.M. *Evaluation of the Induced-Velocity Field of an Idealized Helicopter Rotor*; Wartime
833 Report; UNT: Denton, TX, USA, 1945; p. 28.
- 834 39. Dou, B.; Qu, T.; Lei, L.; Zeng, P. Optimization of wind turbine yaw angles in a wind farm using a three-
835 dimensional yawed wake model. *Energy* **2020**, 118415.
- 836 40. Kuo, J.; Pan, K.; Li, N.; Shen, H. Wind farm yaw optimization via random search algorithm. *Energies* **2020**,
837 *13*, 865.
- 838 41. Porté-Agel, F.; Wu, Y.T.; Chen, C.H. A numerical study of the effects of wind direction on turbine wakes
839 and power losses in a large wind farm. *Energies* **2013**, *6*, 5297–5313

- 840 42. Abkar, M.; Porté-Agel, F. Mean and turbulent kinetic energy budgets inside and above very large wind
841 farms under conventionally-neutral condition. *Renew. Energy* **2014**, *70*, 142–152.
- 842 43. Bastankhah, M.; Porté-Agel, F. A new analytical model for wind-turbine wakes. *Renew. Energy* **2014**, *70*,
843 116–123.
- 844 44. Niayifar, A.; Porté-Agel, F. Analytical modeling of wind farms: A new approach for power prediction.
845 *Energies* **2016**, *9*, 741.
- 846 45. Thomas, J.; Annoni, J.; Fleming, P.; Ning, A. *Comparison of wind farm layout optimization results using a simple
847 wake model and gradient-based optimization to large eddy simulations*; Technical Report; National Renewable
848 Energy Lab. (NREL): Golden, CO(United States), 2019.
- 849 46. Quarton, D.; Ainslie, J. Turbulence in wind turbine wakes. *Wind Energy* **1990**, *14*, 15–23.
- 850 47. Frandsen, S.; Chacen, L.; Crespo, A.; *Measurements on and modeling of offshore wind farms*; Technical Report;
851 Riso National Laboratory: Roskilde, Denmark, 1996.
- 852 48. Frandsen, S.; Thogersen, M.L. Integrated fatigue loading for wind turbines in wind farms by combining
853 ambient turbulence and wakes. *Wind Energy* **1999**, *23*, 327–340.
- 854 49. Kirchner-Bossi, N.; Porté-Agel, F. Realistic wind farm layout optimization through genetic algorithms
855 using a Gaussian wake model. *Energies* **2018**, *11*, 3268.
- 856 50. Turner, S.; Romero, D.; Zhang, P.; Amon, C.; Chan, T. A new mathematical programming approach to
857 optimize wind farm layouts. *Renew. Energy* **2014**, *63*, 674–680.
- 858 51. Jonkman, J.; Butterfield, S.; Musial, W.; Scott, G. *Definition of a 5-MW reference wind turbine for offshore system
859 development*; Technical Report; National Renewable Energy Lab.(NREL): Golden, CO, USA, 2009.
- 860 52. Jonkman, J.; Buhl M. *FAST user's guide*; Technical Report; National Renewable Energy Lab.(NREL): Golden,
861 CO, USA, 2005.
- 862 53. Annoni, J.; Fleming, P.; Scholbrock, A.; Roadman, J.; Dana, S.; Adcock, C.; et al. Analysis of control-oriented
863 wake modeling tools using lidar field results. *Wind Energ. Sci.* **2018**, *3*, 819–831.
- 864 54. Burton, T.; Sharpe, D.; Jenkins, N.; Bossanyi, E. *Wind Energy Handbook*; John Wiley & Sons Ltd.: Chichester,
865 UK, 2001; pp. 35–37. ISBN 0-471-48997-2.
- 866 55. Krogstad, P.A.; Adaramola, M.S. Performance and near wake measurements of a model horizontal axis
867 wind turbine. *Wind Energy* **2012**, *15*, 743–756.
- 868 56. Pedersen, T. On wind turbine power performance measurements at inclined airflow. *Wind Energy* **2004**,
869 *7*, 163–176.
- 870 57. Dahlberg, J.; Montgomerie, B. *Research program of the utgrunden demonstration offshore wind farm*; Technical
871 report; Swedish Defense Research Agency: Kista, Sweden, 2005.
- 872 58. Sørensen, J.N.; Shen, W.Z. Numerical modeling of wind turbine wakes, *J. Fluids Eng.* **2002**, *124*, 393–399.
- 873 59. Churchfield, M.J.; Lee, S.; Michalakes, J.; Moriarty, P.J. A numerical study of the effects of atmospheric and
874 wake turbine dynamics. *J. Turbul.* **2012**, *13*, N14.
- 875

Nomenclature

Variables

x	downstream position from the wind turbine [m]	U_0	incoming wind velocity of the wind farm [m/s]
y	spanwise position from the turbine rotor center [m]	U_w	total streamwise velocity for the combined wake [m/s]
z	vertical position [m]	U_s	total streamwise velocity deficit for the combined wake [m/s]
D	diameter of wind turbine [m]	U_c	mean convection velocity for the combined wake [m/s]
z_h	turbine hub height [m]	V	total transverse velocity for the combined wake [m/s]
		γ_{set}	setting value of the yaw angle [°]

δ	wake center deflection [m]	γ_{added}	added yaw angle [°]
C_T	thrust coefficient	γ_{total}	total yaw angle [°]
C_{T0}	thrust coefficient at zero yaw	U_{equ}	equivalent resultant velocity acting at the rotor plane [m/s]
P	power output	I	turbulence intensity
P_0	power output at zero yaw	I_0	ambient turbulence intensity
k^*	wake width growth rate	I_+	added turbulence intensity
γ	yaw angle [°]	Abbreviations	
u_0	local wind speed perceived by the wind turbine [m/s]	CPV	a counter-rotating vortex pair
u_w	individual streamwise velocity [m/s]	2D	two-dimensional
u_s	individual streamwise velocity deficit [m/s]	3D	three-dimensional
u_c	mean convection velocity for the individual wake [m/s]	SS	sum-of-squares superposition method
v	individual transverse velocity [m/s]	MC	momentum conserving wake superposition method